

N 70 1 15 3  
70-02324  
NASA CR 107350

# STUDIES OF INTERFACE DAMPING

by

U. S. Lindholm  
L. M. Yeakley

## FINAL REPORT

25 November 1966 - 10 September 1969

Contract No. NAS5-10310

SwRI Project No. 02-2033

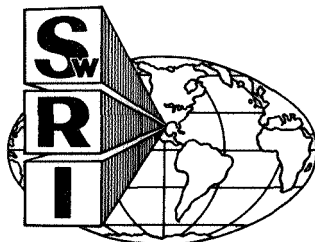
Prepared for

Goddard Space Flight Center  
Greenbelt, Maryland

October 1969



**CASE FILE**  
**COPY**



**SOUTHWEST RESEARCH INSTITUTE**  
SAN ANTONIO                      HOUSTON

SOUTHWEST RESEARCH INSTITUTE  
Post Office Drawer 28510, 8500 Culebra Road  
San Antonio, Texas 78228

# STUDIES OF INTERFACE DAMPING

by

U. S. Lindholm  
L. M. Yeakley

## FINAL REPORT


25 November 1966 - 10 September 1969

Contract No. NAS5-10310  
SwRI Project No. 02-2033

Prepared for  
Goddard Space Flight Center  
Greenbelt, Maryland

October 1969

Approved:

  
on H. Norman Abramson, Director  
Department of Mechanical Sciences

## **ACKNOWLEDGEMENTS**

The authors would like to acknowledge the support of Mr. R. D. Brown in the conduction of the copper friction experiments and also the continued support of Mr. J. P. Young, NASA technical monitor for this program.

## ABSTRACT

The energy dissipation and damping characteristics of aluminum cantilever beams having an interface at which slip is allowed to occur are studied. Theoretical solutions for slip in cantilever beams previously available are extended to beams with either nonsymmetric or multiple interfaces. An approximate solution is obtained in which the effects of distributed inertia forces are included. From forced vibration experiments on beams in air at 1 atmosphere and in vacuum, it is found that the effective coefficient of friction is greater in vacuum. The effect of this increase in friction coefficient on damping, as measured by the loss coefficient, is found to depend upon the vibration amplitude as well as other system parameters.

Supplementary slip experiments with copper show a large increase in friction coefficient in vacuum over that obtained in air.

## TABLE OF CONTENTS

	<u>Page</u>
<b>LIST OF ILLUSTRATIONS</b>	<b>v</b>
<b>I. INTRODUCTION</b>	<b>1</b>
<b>II. ANALYSIS OF INTERFACE SLIP DAMPING IN CANTILEVER BEAMS</b>	<b>3</b>
Static Analysis	3
Nonsymmetric Beam	6
Multiple Interfaces	8
Forced Vibration	9
<b>III. EXPERIMENTS ON INTERFACE SLIP DAMPING IN CANTILEVER BEAMS</b>	<b>15</b>
Procedures	18
Results	20
<b>IV. OSCILLATORY SLIP EXPERIMENTS WITH COPPER</b>	<b>28</b>
<b>V. DISCUSSION</b>	<b>31</b>
<b>VI. CONCLUSIONS</b>	<b>34</b>
<b>VII. REFERENCES</b>	<b>35</b>

## LIST OF ILLUSTRATIONS

<u>Figure</u>		<u>Page</u>
1	Loading and Coordinates for Beam Problem	3
2	Static Load Vs Tip Deflection for Cantilever Beam	5
3a	Loss Factor Vs Load Parameter	6
3b	Loss Factor Vs Displacement Parameter	6
4	Experimental Beam Setup	15
5	Beam Dimensions	16
6	C-Clamps for Control of Clamping Pressure	16
7	Layout of Instrumentation	17
8	Oscilloscope Record of Hysteresis Loop During Forced Vibration of Double Cantilever Beam	18
9	Calibration Curve for Tip Deflection as Measured by Strain Gage at Root of Cantilever Beam	19
10	Photograph Taken at Maximum Dynamic Deflection of Beam Showing Mode Shape and Slip Distribution	19
11	Normalized Static and Dynamic Mode Shapes for Cantilever Beam	21
12	Comparison of Theoretical and Dynamic Experimental Slip Distributions for Cantilever Beam	21
13	Energy Dissipation Vs Tip Deflection for Beams Tested in Air Under Laboratory Conditions	22
14	Energy Dissipation Vs Tip Deflection for Beams Tested in Dry, Hydrocarbon-Free Air	23
15	Energy Dissipation Vs Tip Deflection for Beams Tested in Vacuum ( $\simeq 10^{-9}$ Torr)	24
16	Loss Coefficient Vs Deflection Parameter for All Tests	26
17	Variation of the Apparent First Mode Frequency with the Deflection Parameter $R\nu_m/Q$	26
18	Temperature Rise Measured at the Tip of Cantilever Beam During Steady Vibration	27
19	Energy Dissipation Vs Tangential Force for Copper Tests in Air	29
20	Energy Dissipation Vs Tangential Force for Copper Tests in Vacuum	29
21	Gross Slip Hysteresis Loops for Copper in Air and in Vacuum	30



## I. INTRODUCTION

This report presents results obtained during the second year of a study of interface damping in structural type joints. During the first year of effort, the slip behavior at the interface between two small, nominally flat specimens subject to constant normal load and oscillatory tangential load was studied. Aluminum specimens were tested in atmospheric and vacuum (up to  $10^{-10}$  torr) environments. Differences observed in the slip behavior and energy dissipation between the air and vacuum conditions were attributed to the action of surface oxide layers on the aluminum. These studies were reported in detail in Reference 1.

In the present study, this work is extended to an investigation of the effects of decreasing atmospheric pressure on the magnitude of the energy dissipation or damping in a vibrating structural element. The structure chosen is a cantilever beam having a single interface held together with a constant clamping pressure. This system is amenable to at least approximate analysis of the slip forces and displacements at the interface and, thus, calculation of the energy dissipation per cycle or the loss coefficient. A major objective of the study, then, is an evaluation of the effect of the vacuum environment on the damping properties of this simple structure.

A number of theoretical analyses have been made of the energy dissipation due to slip in various types of lap joints [2,3,4,5]\* and in built-up beams. [6,7,8] These analyses are all based upon the application of a static load cycle, i.e., no inertial forces are considered. A second common assumption is that the slip (relative tangential displacement between the two faces of the joint) is governed by simple Coulomb friction. Thus, slip will occur at any point of the joint interface where the shear stress reaches the critical value

$$\tau_c = \mu \sigma_n \quad (1)$$

where  $\mu$  is the coefficient of Coulomb friction, and  $\sigma_n$  is the stress acting normal to the interface. The coefficient  $\mu$  is taken as a constant, so that differences such as between a static and dynamic coefficient are neglected.

Theoretical analyses of slip damping in built-up beams have been presented by Pian and Hallowell [6], Goodman and Klumpp [7], and Pian [8]. In the investigations of Pian [6,8], a cantilever beam with attached (riveted or bolted) spar caps was considered and analytical solutions derived for the static force-displacement hysteresis loops. For the beam geometries considered, slip was initiated locally at the point of discontinuity between the cap and the beam and the slip area increased continuously with increasing applied load. The analysis of Goodman and Klumpp [7] also considered a cantilever beam; however, the slip area was a continuous interface running the entire length of the beam, i.e., the beam consisted of two identical halves. For this system, slip is not initiated until a finite critical load is applied, then slip occurs simultaneously over the entire interface. Again, static force-displacement relations were derived for this situation. Because of the different manner in which slip is initiated and progresses in the two situations, the analytical solutions are different in form.

Experiments performed using static loading confirmed the shape and magnitude of the predicted hysteresis loops in both cases. In addition, limited dynamic experiments were performed. Pian [8] measured the rate of decay of free vibration. Goodman and Klumpp [7] measured the phase angle between input force and velocity during forced vibration near the first mode fundamental frequency. In both cases, the results of the dynamic experiments appeared to agree in terms of energy dissipation per cycle with the results of the static analysis. These experimental results tend to indicate that the distributed inertia loading and associated changes in mode shape do not significantly change the magnitude of the energy dissipation by slip when compared with an equivalent static loading.

An analysis is available for other types of joints or interfaces; however, it applies generally under direct stress rather than bending stress. See, for instance, the review by Goodman [2] and the recent work on lap joints by Earles

---

\*Numbers in brackets refer to List of References at the end of this report.



[3], Metherell and Diller [4], and Brown [5]. Earles [3] computes the frictional energy dissipation in a simple lap joint with both uniform (constant) and nonuniform clamping pressure, and also for the case where the shear force is partially transmitted by rivets. Metherell and Diller [4] consider uniform clamping pressure only, but calculate the instantaneous rate of energy dissipation in addition to the total dissipation per cycle. Brown [5] considers the geometric and surface factors affecting the interface energy dissipation with regard to optimizing lap joint damping.

Experiments to measure the damping of vibrating cantilever beams in vacuum have been reported by McWithy and Hayduk. [9] Their beams were made of SAE 4130 steel and were riveted or bolted together with a single interface in the configuration analyzed by Goodman and Klumpp. Damping in terms of logarithmic decrement was obtained from the measured decay of tip displacement amplitude after release from a fixed initial amplitude. For low clamping pressure, it was found that the logarithmic decrement increased with tip displacement and was slightly higher in vacuum than in air at atmospheric pressure.

In the succeeding sections of this report, we will first derive the expressions for energy dissipation in a cantilever beam with a single interface under uniform clamping pressure analogous to the solutions of Goodman and Klumpp. [7] The analysis is then extended to the case where the interface may occur at an arbitrary position (two laminates of unequal thickness) and to multiple laminates (interfaces). An approximate analysis including distributed inertia forces is also presented. In Section III, experiments on double cantilever beams under forced vibration are described and compared with analysis. These experiments were run both in vacuum and at atmospheric pressure. Section IV presents some additional slip experiments with small blocks of copper to supplement the aluminum data [1] on a metal with a softer oxide of comparable hardness as the base metal. A discussion of the results obtained and conclusions of the study are presented in Sections V and VI.

## II. ANALYSIS OF INTERFACE SLIP DAMPING IN CANTILEVER BEAMS

The beam configuration being studied has been analyzed by Goodman and Klumpp [7] for a statically applied alternating load by satisfying the two-dimensional stress equilibrium equations and the appropriate stress boundary conditions for each half of the beam. When distributed inertia loading is included in this approach, the resulting plane elasticity problem is not so well posed, as both stress and displacement boundary conditions must be satisfied simultaneously. Initial efforts to solve this two-dimensional dynamic elasticity problem did not suggest that an exact solution was possible. Therefore, the following approximate solution is developed. First, the static solution is derived from essentially one-dimensional, Bernoulli-Euler beam analysis rather than from two-dimensional elasticity theory. This approach gives a little more insight into the mechanics of the problem and leads to a form in which the dynamic correction terms may be included in an approximate manner. The dynamic, forced vibration solution is obtained by adding additional terms arising from the distributed inertia loads to the static displacements. The expressions derived for static loading are, however, the same as obtained in Reference 7.

### Static Analysis

Consider the cantilever beam shown in Figure 1 with thickness  $2h$ , width  $b$ , and length  $l$ . The loading consists of a uniformly distributed clamping pressure  $p$ , and a concentrated load  $P$  applied at the free end,  $x = l$ . Each of the two halves of thickness  $h$  may be considered separately with the loading as depicted in the lower half of Figure 1. The continuity of stress and vertical displacement,  $v$ , is imposed at the interface.

At some finite value of  $P$ , the shear stress at the interface will reach the critical value for slip,  $\tau_{xy} = \mu p$ . Additional loading will then produce a relative displacement  $\Delta u(x)$  at the interface. For completely reversed loading, the product of the shear force,  $\mu p$ , and the relative displacement,  $\Delta u$ , integrated over the length of the beam is equal to one-fourth the energy dissipated in a complete cycle; i.e., the force-relative displacement curve must be symmetric about  $\Delta u = 0$ . Thus, energy dissipation per cycle is given by [7]

$$\begin{aligned} D_s &= 4b \int_0^l \tau_{xy} \Delta u(x) dx \\ &= 4\mu p b \int_0^l (u_2 - u_1) dx \end{aligned} \quad (2)$$

where  $u_1$  and  $u_2$  are the displacements in the  $x$ -direction of points on the adjacent faces of the upper and lower half-beam, respectively. These displacements are produced by the resultant axial force  $F_{1,2}$ , and moment  $M_{1,2}$ , about the centroid of each half-beam. The displacements at any axial position  $x$  and  $y_{1,2} = \mp h/2$  are given by:

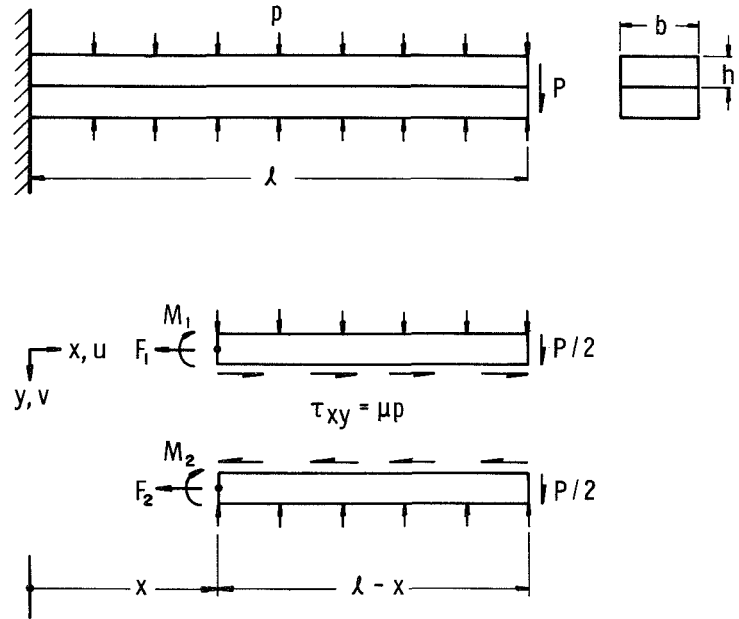


FIGURE 1. LOADING AND COORDINATES FOR BEAM PROBLEM

$$u_1 = \frac{1}{E} \int_0^x \sigma_{x_1} dx' - \frac{h}{2} \frac{dv_1}{dx}$$

and

$$u_2 = \frac{1}{E} \int_0^x \sigma_{x_2} dx' + \frac{h}{2} \frac{dv_2}{dx}$$

(3)

where  $v_1$  and  $v_2$  are the vertical deflections. The continuity condition  $v_1 = v_2 = v$  must prevail.

From simple force equilibrium,

$$\sigma_{x_1} = \frac{\mu p}{h} (l - x); \quad \sigma_{x_2} = -\frac{\mu p}{h} (l - x)$$

(4)

The resultant moment at any section is

$$M_1 = M_2 = \frac{P}{2} (l - x) - \mu p b \frac{h}{2} (l - x)$$

(5)

and the moment-curvature relation yields

$$\frac{d^2 v}{dx^2} = \frac{M}{EI} = \frac{6}{Ebh^3} (P - \mu p b h) (l - x)$$

where  $I = bh^3/12$ . Integrating once gives

$$\frac{dv}{dx} = \frac{6}{Ebh^3} (P - \mu p b h) \left( lx - \frac{x^2}{2} \right) + C_1$$

(6)

where the integration constant  $C_1 = 0$  because of the boundary condition  $(dv/dx)|_{x=0} = 0$ . A second integration yields

$$v = \frac{3}{Ebh^3} (P - \mu p b h) \left( lx^2 - \frac{x^3}{3} \right) + C_2$$

(7)

where again the integration constant  $C_2 = 0$  since  $v|_{x=0} = 0$ . This is the static deflection mode shape,

$$v(x) = \frac{(P - \mu p b h) l^3}{Ebh^3} \left[ 3 \left( \frac{x}{l} \right)^2 - \left( \frac{x}{l} \right)^3 \right]$$

(8)

For convenience, we define two dimensional parameters

$$Q = \mu p b h$$

(9a)

and

$$R = \frac{Ebh^3}{l^3}$$

(9b)

Thus,

$$v(x) = \frac{P - Q}{R} \left[ 3 \left( \frac{x}{l} \right)^2 - \left( \frac{x}{l} \right)^3 \right]$$

(8a)

Combining (3), (4), and (7), and performing the indicated integration, the relative slip displacement at the interface is

$$\Delta u = u_2 - u_1 = \frac{3}{R} \frac{h}{l} \left( P - \frac{4}{3} Q \right) \left[ 2 \left( \frac{x}{l} \right) - \left( \frac{x}{l} \right)^2 \right] \quad (10)$$

Slip will occur only for  $P > P_c = 4Q/3$ . If the beam is loaded cyclically between the loads  $\pm P_m$ , then by substituting (10) in (2) the energy dissipation per cycle is

$$D_s = \frac{8Q}{R} \left( P_m - \frac{4}{3} Q \right) \quad (11)$$

The maximum tip displacement  $v_m$ , corresponding to  $P = P_m$  is obtained from (8) by letting  $x = l$ ;

$$v_m = \frac{2}{R} (P_m - Q) \quad (12)$$

Then the energy dissipation in terms of displacement is

$$D_s = 4Q \left( v_m - \frac{2}{3} \frac{Q}{R} \right) \quad (11a)$$

The load-deflection curve for the beam is given in Figure 2. The curve is bilinear with elastic compliance  $C_1 = 1/2R$ , and slip compliance  $C_2 = 2/R$ . Slip is initiated at the critical load  $P_c = 4Q/3$  and displacement  $v_c = 2Q/3R$ .

In vibration problems, it is most convenient to express the dissipative properties of the system in terms of a nondimensional quantity such as the loss coefficient  $\eta_s$ , defined\* by

$$\eta_s = \frac{D_s}{2\pi U_s} \quad (13)$$

where  $U_s$  is the maximum strain energy stored in the system. The strain energy is

$$U_s = \frac{1}{2} P_m \left( \frac{v_c}{P_c} \right) P_m = \frac{C_1}{2} P_m^2 = \frac{P_m^2}{4R}$$

or

$$U_s = \frac{1}{4R} \left( \frac{Rv_m}{2} + Q \right)^2$$

The following expressions are thus obtained for the loss coefficient:

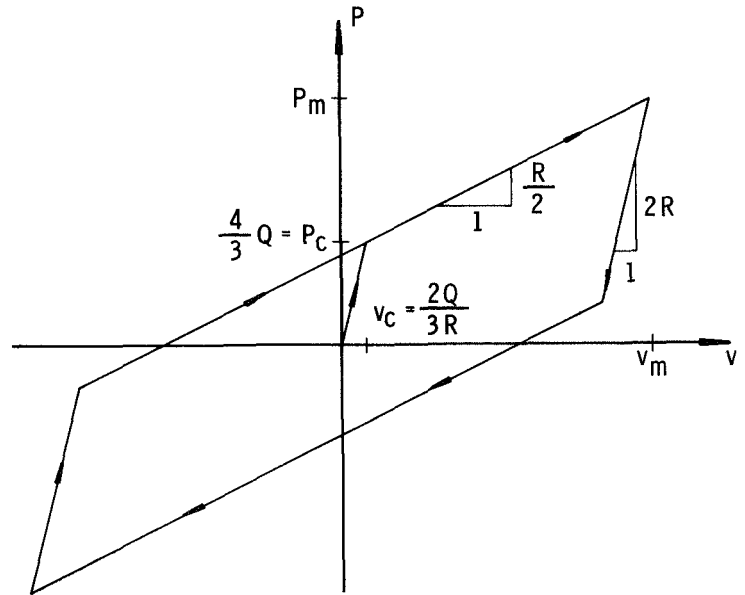


FIGURE 2. STATIC LOAD VS TIP DEFLECTION FOR CANTILEVER BEAM

\*The nomenclature recommended by Lazan [10] is used. Also see Lazan for relationships between  $\eta_s$  and other damping parameters.

$$\eta_s = \frac{32 \left( \frac{Rv_m}{Q} - \frac{2}{3} \right)}{\pi \left( \frac{Rv_m}{Q} + 2 \right)^2} \quad (14a)$$

and

$$\eta_s = \frac{16}{\pi} \left[ \left( \frac{Q}{P_m} \right) - \frac{4}{3} \left( \frac{Q}{P_m} \right)^2 \right] \quad (14b)$$

The relations are plotted in Figures 3a and 3b. The arrows indicate the direction of increasing load or deflection with point A corresponding to the onset of slip. Whereas the energy dissipation per cycle always increases with increasing

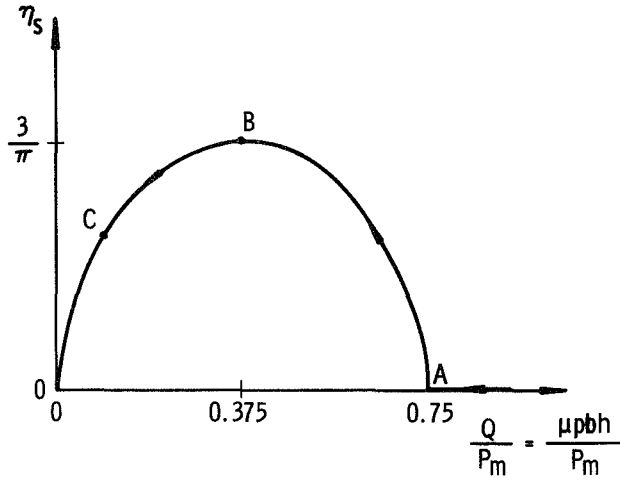


FIGURE 3a. LOSS FACTOR VS LOAD PARAMETER

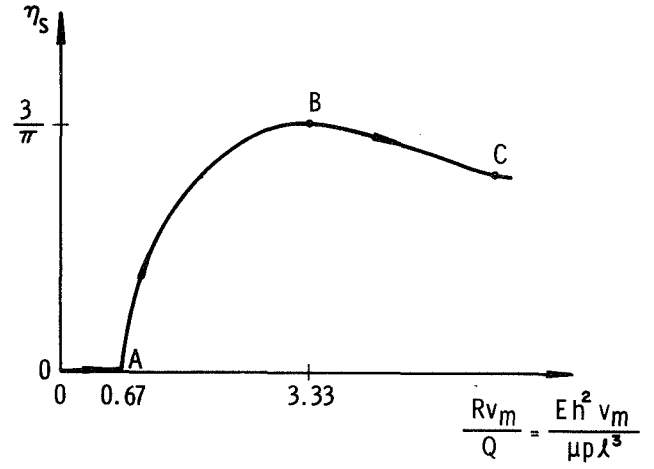


FIGURE 3b. LOSS FACTOR VS DISPLACEMENT PARAMETER

load or deflection, the loss coefficient increases in region AB and then decreases with further increase in load or deflection. The point B at which a maximum in loss coefficient occurs depends upon the values of the dimensional and material parameters of the beam as well as the loading.

### Nonsymmetric Beam

The same analysis may be applied when the two segments of the beam have different thicknesses, say  $h_1$  and  $h_2$ . In this case the interface will not occur at the centroid of the total beam section. Let the total beam thickness again be  $2h$ , so that  $h_1 + h_2 = 2h$ , and let  $h_1 = \alpha h_2$ . Then the stress and moment relations corresponding to (4) and (5) are

$$\sigma_{x_1} = \frac{\mu p(\alpha + 1)}{2\alpha h} \quad (15)$$

$$\sigma_{x_2} = -\frac{\mu p(\alpha + 1)}{2h}$$

and

$$M_1 = P_1(l - x) - \frac{\mu pb\alpha h}{(\alpha + 1)}(l - x) \quad (16)$$

$$M_2 = P_2(l - x) - \frac{\mu pbh}{(\alpha + 1)}(l - x)$$

Integrating the moment relations, the displacements are obtained as

$$v_1 = \frac{3(\alpha + 1)^3}{Ebh^3\alpha^3} \left( P_1 - \frac{\mu pbh\alpha}{(\alpha + 1)} \right) \left( \frac{lx^2}{2} - \frac{x^3}{6} \right) \quad (17)$$

and

$$v_2 = \frac{3(\alpha + 1)^3}{Ebh^3} \left( P_2 - \frac{\mu pbh}{(\alpha + 1)} \right) \left( \frac{lx^2}{2} - \frac{x^3}{6} \right)$$

Enforcing the continuity condition  $v_1 = v_2$  and the relation  $P_1 + P_2 = P$ , we can solve for the loads  $P_1$  and  $P_2$  carried by each beam. Thus

$$P_1 = \frac{\alpha^3 P + \alpha(2\alpha^3 - \alpha + 1)Q}{\alpha^3 + 1} \quad (18)$$

$$P_2 = \frac{P + \alpha(\alpha - 1)Q}{\alpha^3 + 1}$$

Utilizing (15), (16), and (17) in (3) and (2), and carrying out the indicated operations and algebra, one arrives at the relations for energy dissipation:

$$D_s = \frac{2(\alpha + 1)^3}{(\alpha^3 + 1)} \frac{Q}{R} \left[ P_m - \frac{(\alpha^3 + 3\alpha^2 + 3\alpha + 1)}{3\alpha(\alpha + 1)} Q \right] \quad (19)$$

or

$$D_s = 4Q \left[ v_m - \frac{(\alpha + 1)^2}{6\alpha} \frac{Q}{R} \right]$$

where  $Q$  and  $R$  are defined as before [(9a) and (9b)]. Correspondingly the loss coefficient is

$$\eta_s = \frac{32 \left[ \frac{Rv_m}{Q} - \frac{(\alpha + 1)^2}{6\alpha} \right]}{\pi \left[ \frac{Rv_m}{Q} + 2 \right]^2} \quad (20)$$

For  $\alpha = 1$ , (19) and (20) reduce to (11) and (14). All other parameters remaining constant, for  $\alpha > 1$ , initiation of slip requires a larger displacement and the maximum in the loss coefficient is decreased in comparison with  $\alpha = 1$ . In other words, energy dissipation vs damping is maximized by having the slip surface at the centroid of the total beam cross section.

## Multiple Interfaces

Consider the beam made up of three laminates of equal thickness, so that slip is occurring on two interfaces simultaneously. Again, for comparative purposes, let the total thickness of the beam be  $2h$ , and the thickness of each laminate is then  $2h/3$ . For the two outer laminates (denoted by subscripts 1 and 3), the displacements at the interface  $y = \mp h/3$  are

$$u_{1,3} = \frac{1}{E} \int_0^x \sigma_{x1,3} dx \mp \frac{h}{3} \frac{dv}{dx}$$

and for the center laminate (subscript 2)

$$u_2 = \pm \frac{h}{3} \frac{dv}{dx}$$

Because the shear loading on the center laminate is balanced, the axial stress resultant  $\sigma_{x2} = 0$ . The other stress resultants are

$$\sigma_{x1} = \frac{3\mu p}{2h} (l - x)$$

$$\sigma_{x3} = -\frac{3\mu p}{2h} (l - x)$$

The bending moments are

$$M_1 = M_3 = P_{1,3}(l - x) - \mu p b \frac{h}{3} (l - x)$$

and

$$M_2 = P_2(l - x) - \mu p b \frac{2h}{3} (l - x)$$

From the moment relations, the vertical displacements are found to be

$$v_{1,3} = \frac{27}{2Ebh^3} (3P_{1,3} - \mu p b h) \left( \frac{lx^2}{2} - \frac{x^3}{6} \right)$$

and

$$v_2 = \frac{27}{2Ebh^3} (3P_2 - 2\mu p b h) \left( \frac{lx^2}{2} - \frac{x^3}{6} \right)$$

Requiring that  $v_1 = v_2 = v_3$  and  $P_1 + P_2 + P_3 = P$  determines:

$$P_1 = P_3 = \frac{1}{3} \left( P - \frac{1}{3} Q \right)$$

and

$$P_2 = \frac{1}{3} \left( P - \frac{2}{3} Q \right)$$

The energy dissipation is then determined directly from (2) by summing the slip displacements over the two interfaces. Performing the required operations leads to

$$D_s = \frac{24Q}{R} \left( P_m - \frac{3}{2} Q \right)$$

and

(21)

$$D_s = \frac{16Q}{3} \left( v_m - \frac{3}{4} \frac{Q}{R} \right)$$

The loss coefficient is

$$\eta_s = \frac{128}{3\pi} \frac{\left[ \frac{Rv_m}{Q} - \frac{3}{4} \right]}{\left[ \frac{Rv_m}{Q} + 2 \right]^2} \quad (22)$$

For the same total thickness beam, the maximum in the loss coefficient is increased approximately 30 percent by having three rather than two equal laminates. However, for three laminates the onset of slip is delayed to higher load,  $P_c = 3Q/2$  because the slip interface is off the center of the beam. This same critical load can be obtained by using  $\alpha = 2$  in (19).

Additional numbers of laminates may be handled in a similar fashion. However, since slip will occur sequentially on each interface depending upon its distance from the center of the total beam section, the load deflection curve will become piece-wise linear instead of bilinear as in the examples cited thus far. It is also possible to include laminates of different material or modulus.

## Forced Vibration

For the forced vibration of a cantilever beam, it is necessary to extend the static analysis to include distributed inertia forces and examine their effect on the mode shape, slip distribution and energy dissipation due to slip. The analysis developed here will follow the static analysis developed in the preceding sections for the beam as shown in Figure 1.

We will consider the forced vibration of the beam produced by a time-dependent displacement at the unsupported end such that

$$v|_{x=l} = f(t)$$

Following Timoshenko [11], the dynamic displacement may be composed of two parts

$$v = v_I + v_{II}$$



where

$$v_I = \left[ \frac{3}{2} \left( \frac{x}{l} \right)^2 - \frac{1}{2} \left( \frac{x}{l} \right)^3 \right] f(t) \quad (23)$$

The term in brackets represents the static mode function and satisfies the end conditions:

$$v_I|_{x=0} = 0 ; \quad \frac{dv_I}{dx} \Big|_{x=0} = 0 ; \quad \frac{d^2 v_I}{dx^2} \Big|_{x=l} = 0 ; \quad v_I|_{x=l} = f(t) \quad (24)$$

but not the dynamic equilibrium equation

$$EI \frac{\partial^4 v}{\partial x^4} + \rho A \frac{\partial^2 v}{\partial t^2} = 0 \quad (25)$$

The displacements  $v_I$  produce dynamic loads given by

$$-th\rho \left[ \frac{3}{2} \left( \frac{x}{l} \right)^2 - \frac{1}{2} \left( \frac{x}{l} \right)^3 \right] \ddot{f}(t) \quad (26)$$

Therefore, the displacements  $v_{II}$  must satisfy the end conditions

$$v_{II}|_{x=0} = 0 ; \quad \frac{dv_{II}}{dx} \Big|_{x=0} = 0 ; \quad \frac{d^2 v_{II}}{dx^2} \Big|_{x=l} = 0 ; \quad v_{II}|_{x=l} = 0 \quad (27)$$

and represent vibrations produced by the forcing function (26). We thus take

$$v_{II} = \sum_i \varphi_i(t) X_i(x) \quad (28)$$

where the modal functions  $X_i$  are solutions of (25) and satisfy the end conditions (27). Thus,

$$X_i = \sinh k_i l \sin k_i(l - x) - \sin k_i l \sinh k_i(l - x) \quad (29)$$

where  $k_i$  are the roots of

$$\tanh k_i l = \tan k_i l \quad (30)$$

The total displacement is then

$$v = \left[ \frac{3}{2} \left( \frac{x}{l} \right)^2 - \frac{1}{2} \left( \frac{x}{l} \right)^3 \right] f(t) + \sum_i \varphi_i(t) X_i(x) \quad (31)$$

By application of the principle of virtual work, it is straightforward to show [11] that the time-dependent functions  $\varphi_i(t)$  must satisfy the differential equation

$$\ddot{\varphi}_i + \frac{EI k_i^4}{A\rho} \varphi_i = -b_i \ddot{f}(t) \quad (32)$$

where the dot superscripts denote differentiation with respect to time. The coefficients  $b_i$  are obtained by expanding the forcing function (26) in a series of the normal functions,  $X_i$ . Thus,

$$-A\rho\ddot{f}(t)\left[\frac{3}{2}\left(\frac{\dot{x}}{l}\right)^2 + \frac{1}{2}\left(\frac{x}{l}\right)^3\right] = -A\rho\ddot{f}(t) \sum_i b_i X_i$$

and the coefficients  $b_i$  are obtained from

$$b_i = \frac{\int_0^l X_i \left[ \frac{3}{2} \left( \frac{x}{l} \right)^2 - \frac{1}{2} \left( \frac{x}{l} \right)^3 \right] dx}{\int_0^l X_i^2 dx}$$

Upon performing the indicated integrations, it is found that

$$b_i = \frac{2}{k_i l (\sinh k_i l - \sin k_i l)} \quad (33)$$

The general solution of (31) is

$$\varphi_i(t) = A_i \cos p_i t + B_i \sin p_i t - \frac{b_i}{p_i} \int_0^t \ddot{f}(\tau) \sin p_i(t - \tau) d\tau \quad (34)$$

where

$$p_i = \left( \frac{EI}{A\rho} \right)^{1/2} k_i^2$$

We now evaluate the  $A_i$  and  $B_i$  from the initial conditions

$$\begin{aligned} v(0) &= U(x,0) \\ \dot{v}(0) &= V(x,0) \end{aligned} \quad (35)$$

From (31) and (35)

$$U = \left[ \frac{3}{2} \left( \frac{x}{l} \right)^2 - \frac{1}{2} \left( \frac{x}{l} \right)^3 \right] f(0) + \sum_i X_i \{A_i\}$$

and

$$V = \left[ \frac{3}{2} \left( \frac{x}{l} \right)^2 - \frac{1}{2} \left( \frac{x}{l} \right)^3 \right] \dot{f}(0) + \sum_i X_i \{B_i p_i\}$$

However, since:

$$\left[ \frac{3}{2} \left( \frac{x}{l} \right)^2 - \frac{1}{2} \left( \frac{x}{l} \right)^3 \right] = \sum_i b_i X_i$$

$$U(x,0) = \sum_i X_i \left\{ A_i + b_i f(0) \right\}$$

$$V(x,0) = \sum_i X_i \left\{ B_i p_i + b_i \dot{f}(0) \right\}$$

Taking initial conditions  $U = V = 0$ , we have

$$A_i = -b_i f(0)$$

$$B_i = -\frac{b_i}{p_i} \dot{f}(0) \quad (36)$$

Substitution of (36) and (34) into (31), yields

$$\begin{aligned} v(x,t) = & \left[ \frac{3}{2} \left( \frac{x}{l} \right)^2 - \frac{1}{2} \left( \frac{x}{l} \right)^3 \right] f(t) - f(0) \sum_i b_i X_i \cos p_i t \\ & - \dot{f}(0) \sum_i \frac{b_i}{p_i} X_i \sin p_i t - \sum_i \frac{b_i}{p_i} X_i \int_0^t \ddot{f}(\tau) \sin p_i(t-\tau) d\tau \end{aligned} \quad (37)$$

Using,

$$\begin{aligned} \int_0^t \ddot{f}(\tau) \sin p_i(t-\tau) d\tau = & -\dot{f}(0) \sin p_i t + p_i f(t) - p_i f(0) \cos p_i t \\ & - p_i^2 \int_0^t f(\tau) \sin p_i(t-\tau) d\tau \end{aligned}$$

(37) becomes

$$\begin{aligned} v(x,t) = & \left[ \frac{3}{2} \left( \frac{x}{l} \right)^2 - \frac{1}{2} \left( \frac{x}{l} \right)^3 \right] f(t) - \sum_i b_i X_i f(t) \\ & + \sum_i b_i X_i p_i \int_0^t f(\tau) \sin p_i(t-\tau) d\tau \end{aligned} \quad (38)$$

The relative slip at the interface is given by

$$\Delta u_x = u_2 - u_1 = -\frac{\mu p l^2}{E h} \left( \frac{2x}{l} - \frac{x^2}{l^2} \right) + h \frac{dv}{dx} \quad (39)$$

Utilizing the mode shape (38), (39) becomes:

$$\begin{aligned}
\Delta u = & \left[ -\frac{\mu p l^2}{Eh} + \frac{3h}{2l} f(t) \right] \left( \frac{2x}{l} - \frac{x^2}{l^2} \right) \\
& + h \sum_i b_i k_i [\sinh k_i l \cos k_i(l-x) - \sin k_i l \cosh k_i(l-x)] \\
& \times [f(t) - p_i \int_0^t f(\tau) \sin p_i(t-\tau) d\tau]
\end{aligned} \tag{40}$$

Equations (38) and (40) account for the effect of distributed inertial forces on the transverse mode shape and relative slip distribution.

The change in the distribution of slip due to the dynamic terms will now be shown not to effect the energy dissipation per cycle. The energy dissipation is again given by the product of the interface shear stress (assumed constant during slip) and the relative slip integrated over the length of the beam according to (2). Using (40) and performing the integration, there results

$$D_s = 4\mu p b h \left[ f(t) - \frac{2}{3} \frac{\mu p l^2}{Eh^2} \right] \tag{41}$$

where  $f(t)$  must be interpreted as the maximum oscillatory amplitude of the tip displacement. This result is the same as obtained for a static tip displacement,  $v_m$ . The second or dynamic term in (40) makes no contribution. This can be understood by examining the relation (39). Changes in the dynamic mode shape  $v(x)$  enter the energy dissipation relation (2) through the term

$$\begin{aligned}
\int_0^l \frac{\partial v}{\partial x} dx &= v|_{x=l} - v|_{x=0} \\
&= v_I|_{x=l} + \cancel{v_{II}|_{x=l}}^0 - \cancel{v_I|_{x=0}}^0 - \cancel{v_{II}|_{x=0}}^0
\end{aligned}$$

From the boundary conditions (24) and (27), all displacements except  $v_I|_{x=l}$  corresponding to the static mode shape vanish. Thus, while the distribution of slip is changed, the total integrated slip is the same for equal static and dynamic tip displacements.

The dynamic analysis above can be considered only approximate when slip is occurring, since the system is then nonlinear, having a nonconstant compliance or stiffness. The dynamic analysis is based upon linear vibration theory. A more exact analysis would require the inclusion of amplitude dependent, in-plane shear forces or equivalent axial stress resultants. The inclusion of distributed forces along the length of the beam also implies that the shear stress at the interface is not constant as in the static case. Therefore, the transition from the fully elastic region to the region where slip is occurring may be expected to be somewhat gradual in the dynamic case rather than abrupt as in the static case. For the fundamental mode, where the static and dynamic mode shapes do not differ greatly, it would appear that the static analysis will be sufficiently accurate to predict energy dissipation. This is partially substantiated by the experiments [7,8] mentioned previously.

Since the force-displacement curve (Figure 2) is nonlinear and hysteretic, it is possible to only estimate a frequency corresponding to a fundamental resonant mode. This frequency will be amplitude dependent. An approximate expression for the fundamental frequency of a cantilever beam is

$$f_1 = \frac{1}{2\pi} \left[ \frac{K}{0.23M} \right]^{1/2}$$

where  $f_1$  is the frequency in cps,  $K$  is an effective static stiffness and  $M = 2lbh\rho$  is the total mass of the beam. For the cantilever beam with a single, central interface, we can let

$$K = \frac{P_m}{v_m} = \frac{Eb h^3}{2l^3} + \frac{\mu p b h}{v_m}$$

then

$$f_1 = 0.166 \left[ \frac{Eh^2}{l^4 \rho} + \frac{2\mu p}{l \rho v_m} \right]^{1/2} ; \quad v \geq v_c$$

Rearranging and letting  $c_o = (E/\rho)^{1/2}$ , we obtain

$$\frac{6l^2}{hc_o} f_1 = \left[ 1 + \frac{2Q}{Rv_m} \right]^{1/2} ; \quad v \geq v_c \quad (41)$$

The frequency parameter  $(6l^2/hc_o)f_1$  varies between the limits 1 and 2. The maximum frequency, corresponding to a solid beam of thickness  $2h$  is obtained by setting  $v_m = v_c = 2Q/3R$ . The minimum frequency occurs when  $Q = 0$  and two beams of thickness  $h$  vibrate independently.

### III. EXPERIMENTS ON INTERFACE SLIP DAMPING IN CANTILEVER BEAMS

#### Apparatus

The experimental setup consists of a double cantilever beam driven by an electromagnetic exciter as shown in Figure 4. A similar arrangement was used by Granick and Stern [12] for the measurement of material damping in solid beams. In the present system, energy dissipation is obtained from direct measurement of the input force and displacement. The energy supplied at the input point can be dissipated by slip at the interfaces of the beam, hysteretic losses due to cyclic stress in the beam, and by losses due to interaction of the beam with the surrounding atmosphere. It will be shown in Section V that the measured losses are due almost entirely to slip.

The major parts of the system can be seen in Figure 4. The 50-lb capacity electromagnetic exciter is rigidly attached to a flange which mounts on one port of the vacuum facility. The vacuum facility is the same as described in Reference 1. The exciter drives the midpoint of the double cantilever beam through a carefully guided shaft. The length of the driving shaft is such as to position the beam in the vacuum facility at a point where it can be visually observed through a viewing port. A flexible bellows connects the mounting flange and the driving shaft to provide a vacuum seal for the externally mounted exciter.

The input driving force is measured by a strain gage instrumented dynamometer section in series with the drive shaft and the beam. The input displacement is measured by a noncontacting, inductance type displacement transducer, rigidly mounted to the base and positioned to measure the displacement of the midpoint of the beam.

The composite beam is constructed of two identical halves held together with periodically spaced clamps. The clamping arrangement is similar to that of Reference 7. The dimensions of the beams and clamps are given in the drawings of Figures 5 and 6. The beams are made of 7075-T6 aluminum and the interface surface is machined flat with a single-point flycutter on a milling machine. The surfaces were prepared in the same manner as in previous experiments reported in Reference 1.

The C-type clamps provide variable clamping pressure by adjustment of the screw which applies the normal load. The load applied by each clamp is determined by a strain gage mounted on the back of each clamp. The output from each strain gage (clamp) was calibrated in terms of clamping force by means of dead-weight loading of the clamp. The strain gages on the clamps also allow monitoring of the dynamic clamping pressure during vibration of the beam. Since

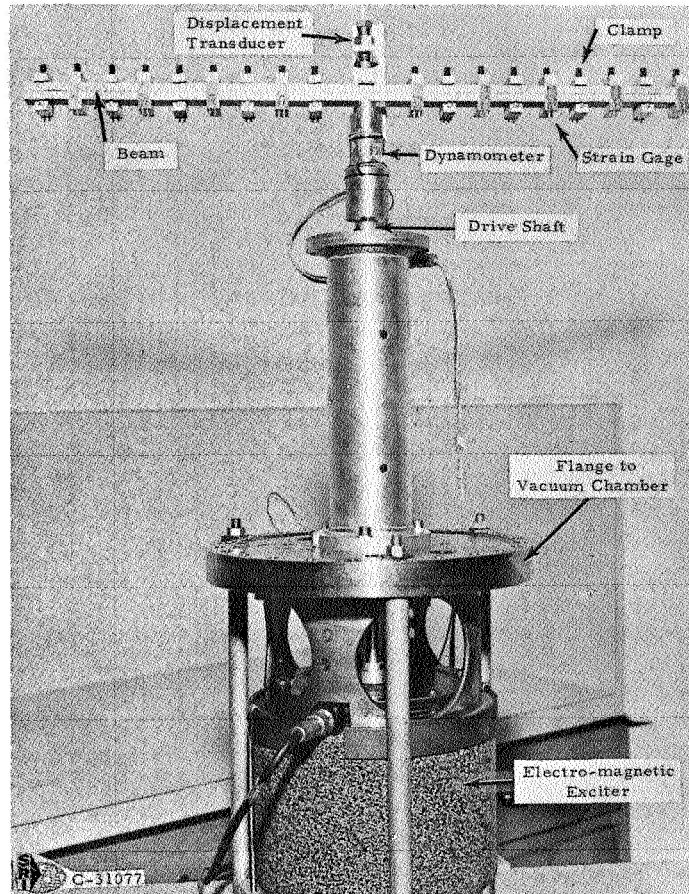
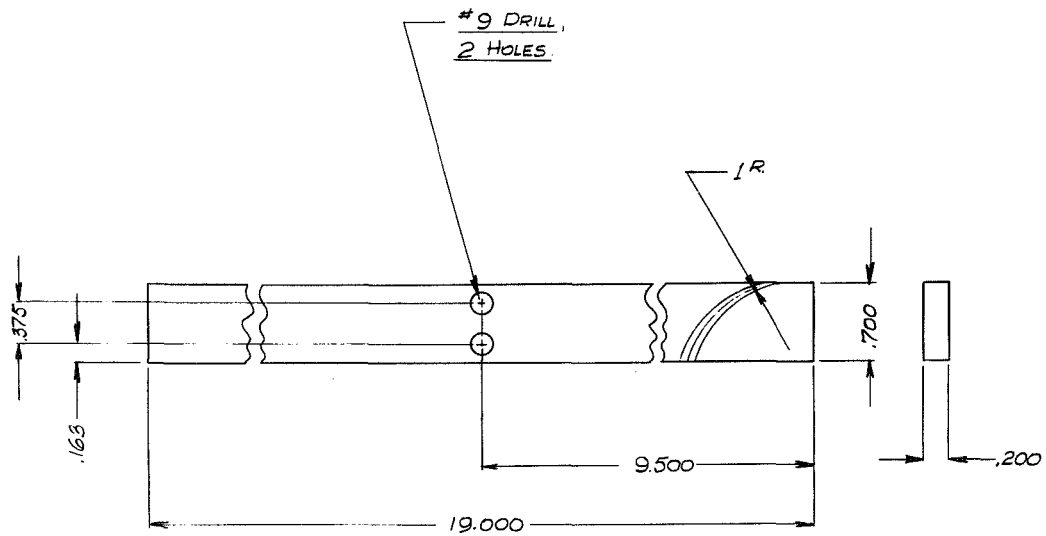
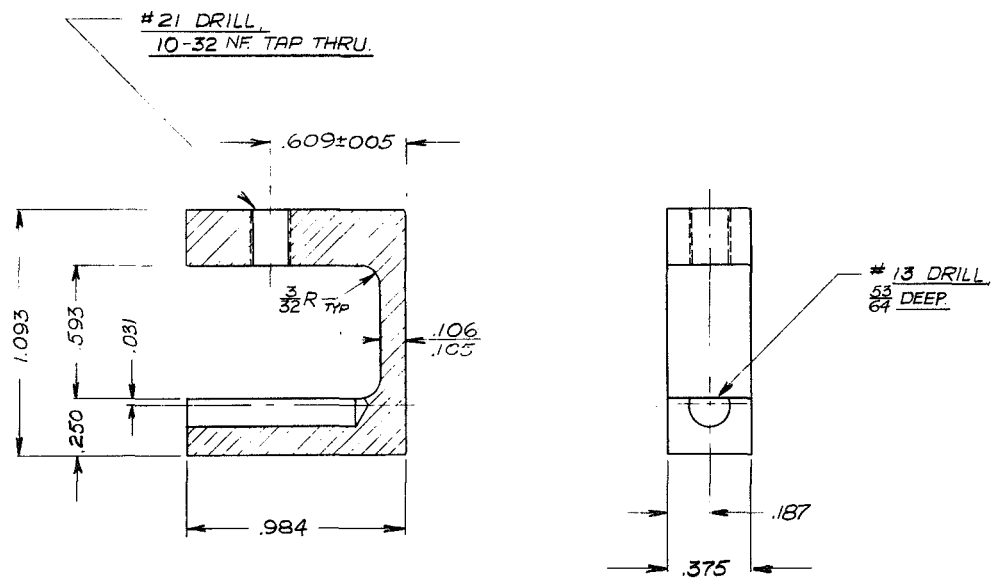


FIGURE 4. EXPERIMENTAL BEAM SETUP



FLY CUT TO PATTERN SHOWN.

FIGURE 5. BEAM DIMENSIONS



NOTE: BREAK SHARP EDGES!

FIGURE 6. C-CLAMPS FOR CONTROL OF CLAMPING PRESSURE

the clamp must rotate slightly to accommodate displacement of the beam during bending, the dynamic clamping pressure oscillates about the mean (static) pressure at twice the input driving frequency. This variation has been measured to be approximately 5 percent of the mean value, depending upon the displacement amplitude, but will be assumed to have small effect upon the dissipation characteristics. Actually, since the clamps are at discrete points, there will be spatial as well as time-wise variations in clamping pressure at the interface. The beams were purposely made relatively thick in order to help distribute the normal pressure uniformly at the interface.

The signal processing and recording instrumentation are shown schematically in Figure 7. The complete force-displacement hysteresis loop is displayed directly on an oscilloscope with photographic records taken as required. A

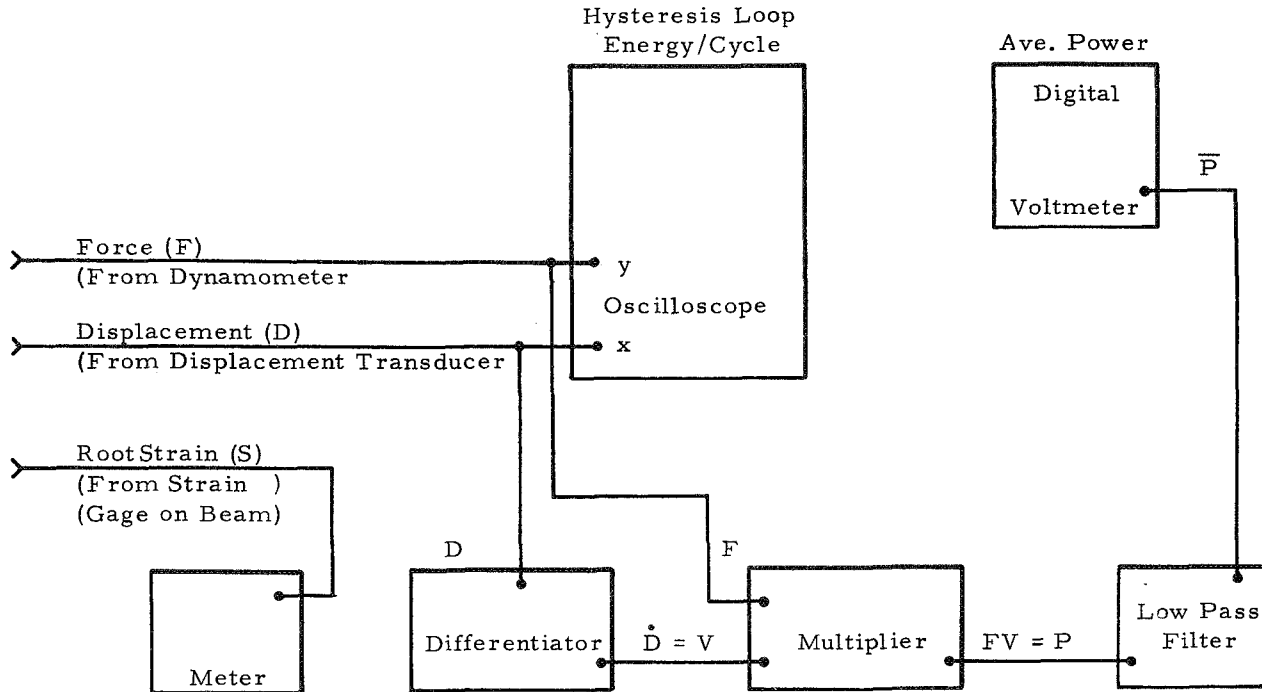


FIGURE 7. LAYOUT OF INSTRUMENTATION

typical scope record of a hysteresis loop is shown in Figure 8. This loop is characteristic of the loops obtained in both vacuum and air and corresponds to the theoretical shape shown in Figure 2. The static force displacement curve for the composite beam is bilinear with a change in compliance at the onset of slip of 4 to 1. This bilinear behavior results in harmonics in the forced vibration response, as evidenced by the oscillations observable in the hysteresis loop record. The energy dissipated per cycle may be obtained directly from this record by integrating the area within the hysteresis loop. A more direct method of average power measurement is made electronically by multiplying the input force and velocity signals and recording the output on a digital voltmeter. The velocity is obtained by electronically differentiating the displacement-time signal. From the measured power,  $Q$ , and frequency,  $f$  (in cps), the energy loss per cycle is obtained from  $D_s = Q/f$ . This direct power measurement is more convenient than the measurement of the hysteresis loop without loss in accuracy.

As noted by Granick and Stern [12], there are two closely spaced frequencies at which the double cantilever beam may be excited. One frequency corresponds to a relative maximum in the input force and a minimum displacement at the driving point. The second frequency corresponds to a relative minimum in the input force and large input displacement. The normalized mode shape of the beam relative to the root is the same at both frequencies as determined by dynamic measurements. The bulk of the test data was obtained at the frequency corresponding to a



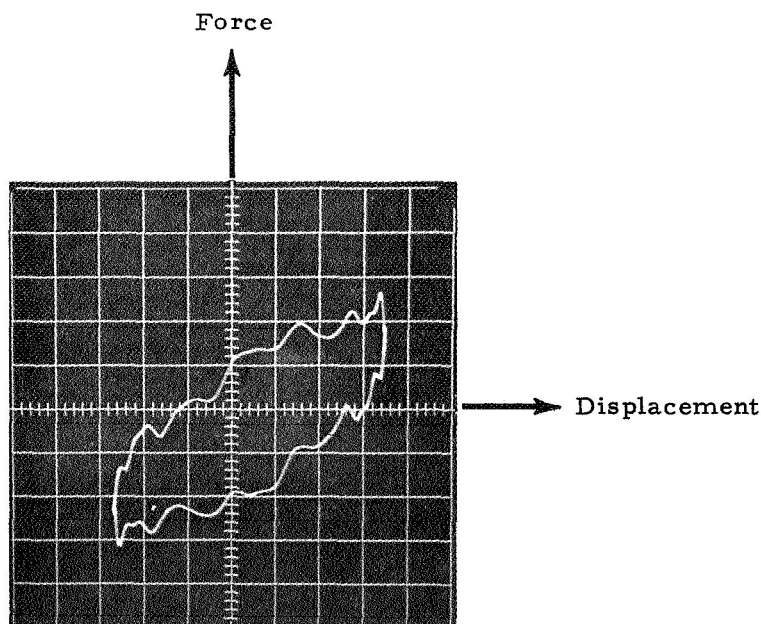


FIGURE 8. OSCILLOSCOPE RECORD OF HYSTERESIS LOOP DURING FORCED VIBRATION OF DOUBLE CANTILEVER BEAM

minimum in the input force. This allowed us to achieve relatively large tip displacements within the force capacity of the electromagnetic exciter.

The tip amplitude,  $v_m$ , which was used as a control variable, was determined from strain amplitude readings taken from near the root of the beam by means of resistance strain gages. Assuming the static mode shape, as given by (8a), the strain at the outer surface of the beam can be shown to be given by

$$\epsilon_x = \frac{3}{2} \frac{h}{l^2} v_m + \frac{\mu p l}{E h} \left( 1 - \frac{x}{l} \right)$$

when  $v_m \geq v_c$ , and

$$\epsilon_x = \frac{3h}{l^2} v_m \left( 1 - \frac{x}{l} \right)$$

when  $v_m \leq v_c$ . When slip is occurring, the slope  $dv_m/d\epsilon$  is twice the slope for the rigid beam. A calibration curve for strain vs tip displacement is given in Figure 9 illustrating the predicted behavior. The calibration slope  $dv_m/d\epsilon$  varies by 18 percent from that predicted from the static mode shape. Since the strain depends upon the second derivative of  $v(x)$ , this difference is not surprising.

In preliminary tests, the mode shape, tip displacement, and relative slip were measured photographically. This was done by using a strobe light synchronized to the frequency of the beam to "stop" the motion for a photographic record. A horizontal and vertical grid was ruled on the side of the beam so that absolute displacements could be measured from the photograph. A typical photograph of the beam during vibration is shown in Figure 10.

## Procedures

Tests were performed under three separate environmental conditions, with three beam specimens tested for each condition. These conditions were:

- (1) Ambient room air at 1 atm pressure, beam surfaces cleaned only with acetone.
- (2) Dry air at 1 atm pressure, beam surfaces carefully cleaned by vapor degreasing.
- (3) Vacuum ( $\approx 10^{-9}$  torr), beam surfaces carefully cleaned by vapor degreasing.

For the first condition, the tests were performed in the open laboratory. Both the second and third test conditions were achieved with the beam sealed in the vacuum chamber. The dry air had less than 2 ppm hydrocarbons. The surface cleaning procedure for the dry air and vacuum tests was as follows:

- (1) Vapor degreasing in trichloroethylene
- (2) Immersion for 3 min in caustic solution (8 g sodium carbonate, 6 g trisodium phosphate, and water to 1 liter) at 170-200°F.

- (3) Rinsing with hot water
- (4) Immersion for 3 min in acid solution (60 g chromic acid, 160 cc sulfuric acid, and water to 1 liter) at 110-180°F.
- (5) Rinsing with hot water.

Surfaces cleaned by this technique were sufficiently clean to be "wet" by water.

The purpose of the three test conditions was to determine their effect upon the energy dissipation of the beam system during forced oscillation. Each beam was allowed to vibrate for at least 20 min at a maximum tip amplitude of 0.25 in. before taking readings at each test condition. Measurements were then taken of power, frequency, input force and displacement, and root strain. Two readings were taken at each tip displacement (strain) amplitude, one while the displacement was being incrementally increased and a second while it was being decreased. While there were often differences in these two readings, the magnitudes could not be associated with the direction of the loading cycle.

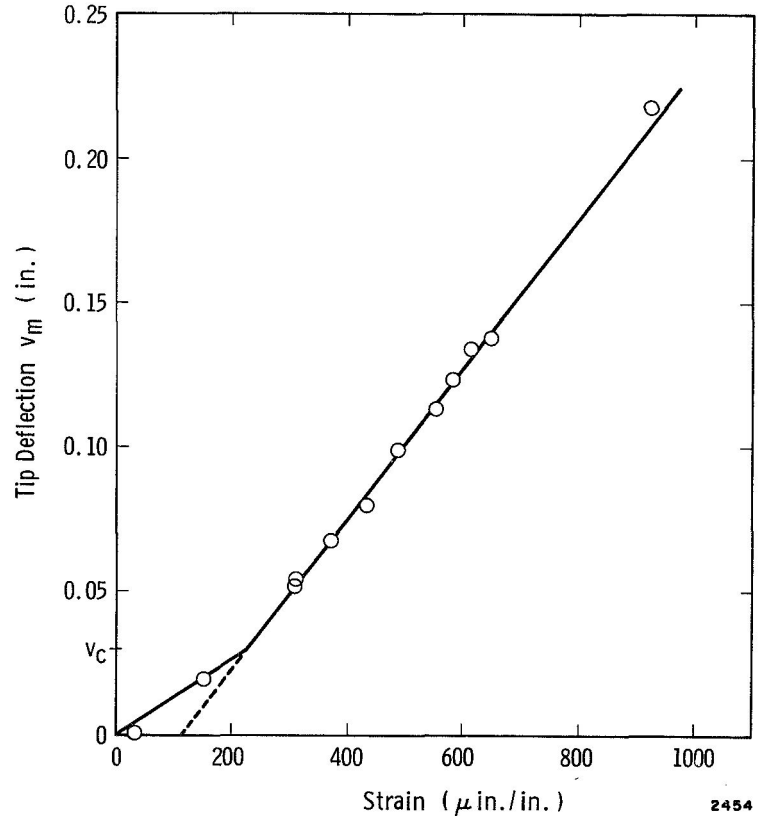


FIGURE 9. CALIBRATION CURVE FOR TIP DEFLECTION AS MEASURED BY STRAIN GAGE AT ROOT OF CANTILEVER BEAM

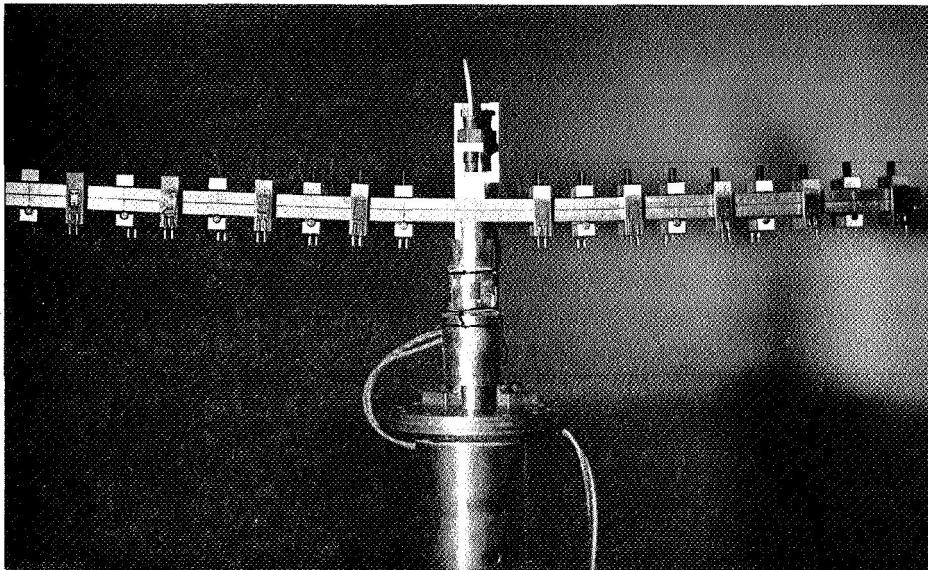


FIGURE 10. PHOTOGRAPH TAKEN AT MAXIMUM DYNAMIC DEFLECTION OF BEAM SHOWING MODE SHAPE AND SLIP DISTRIBUTION

The tests were repeated at three clamping pressures, 10, 20, and 30 psi. The clamping pressure was read from the strain gages on each clamp at both the beginning and at the end of the test. These clamping pressures were never found to change more than 5 percent from their initial values. The same beam was tested at each clamping pressure, starting with the lowest value and then resetting the clamps to the next higher pressure. Otherwise, new beam specimens were used for each test.

## Results

From photographic records such as Figure 10, the mode shapes and slip distributions were obtained for several beams in air in the laboratory. These were used to confirm the modal distributions of (8) and (10). The normalized transverse displacement,  $v_m$ , is given in Figure 11 for both static and dynamic loading. The dynamic mode shapes were obtained for both modes where the input force is either maximum or minimum. In the normalized displacement  $(v - D)/v_m$ , the rigid body displacement,  $D$ , is subtracted out. There is little difference in the measured mode shapes and they all agree reasonably with the theoretical static mode shape.

The slip displacement is given in Figure 12. Again, there is reasonable agreement between the experimental dynamic measurements and the theoretical static distribution. The maximum magnitude of the slip displacement, which occurs at  $x = l$ , ranges from 0.001 to 0.01 in. for the range of experimental conditions included in the test program.

The magnitude of the energy dissipation per cycle calculated from the experimental measurements are plotted in Figures 13, 14, and 15 for the air, dry air, and vacuum tests, respectively. The experimental values have been divided by two to correspond to the single cantilever beam of the analysis. Each plot contains data points from three beams, each beam tested at three different values of clamping pressure. The solid lines drawn through the data points are a fit to the data based upon (11a) and the indicated value of coefficient of friction  $\mu$ . It should be noted that  $\mu$ , which is treated as the only unknown parameter in (11a), is determined from both the zero intercept of the curve,  $v_c = 2Q/3R = 2/3 [( \mu p l^3 ) / ( E h^2 )]$ , and the slope of the curve,  $dD_s/dv_m = 4Q = 4\mu p b h$ .

While the scatter, or nonrepeatability, of the data in some cases is appreciable, the behavior of the system is in general agreement with the theory as developed. The scatter appears to be due to the lack of reproducibility of the interface conditions, even after careful preparation, rather than a systematic deviation from the slip mechanism assumed in the development of the theory. Much of the scatter could be accounted for by assuming a different coefficient of friction for each individual specimen, rather than averaging three specimens at each clamping pressure. Only for a few specimens in vacuum was the data for a given specimen clearly nonlinear over the range in displacement. In these cases, the coefficient of friction was apparently decreasing with increasing tip displacement amplitude.

The coefficients of friction  $\mu$ , obtained from the data of Figures 13-15, are summarized in Table I. Even for a given environmental condition, there appears to be some variation in the coefficient with clamping pressure. Some of this variation, such as for vacuum, is within the scatter of the individual data and may not be significant. However, in air, where the data are most reproducible, the differences are not within the scatter of the data. Thus, there appears to be some effect of clamping pressure on coefficient of friction for the particular surfaces studied. Goodman and Klumpp [7], whose tests covered an even wider range in clamping pressure, found the coefficient to be constant. Their surfaces, however, were specially prepared and lubricated with  $\text{MoS}_2$  and oil so as to control the friction coefficient.

More significant than the changes in friction coefficient with clamping pressure is the larger increase in  $\mu$  when going from air at 1 atmosphere to carefully cleaned surfaces in a vacuum. The coefficient of friction is roughly doubled in vacuum over its value in room air with surface conditions which would approximate typical assembly practices. Removing the moisture from the air and contaminants from the surfaces of the metal tends to increase  $\mu$ , as expected, but not to the same extent as the vacuum. As in the previous study with aluminum [1], the explanation appears to involve the role played by the hard surface oxide layers. In air, the oxide layer is continuously replenished if it is mechanically removed by the fretting action of the slip. Oxide debris particles are evident at the interface even after short periods of vibration. In vacuum, the oxide layer, once it is mechanically removed from the asperity points of contact, is not renewed and metal contact is established. This enhances the adhesion between the two surfaces and

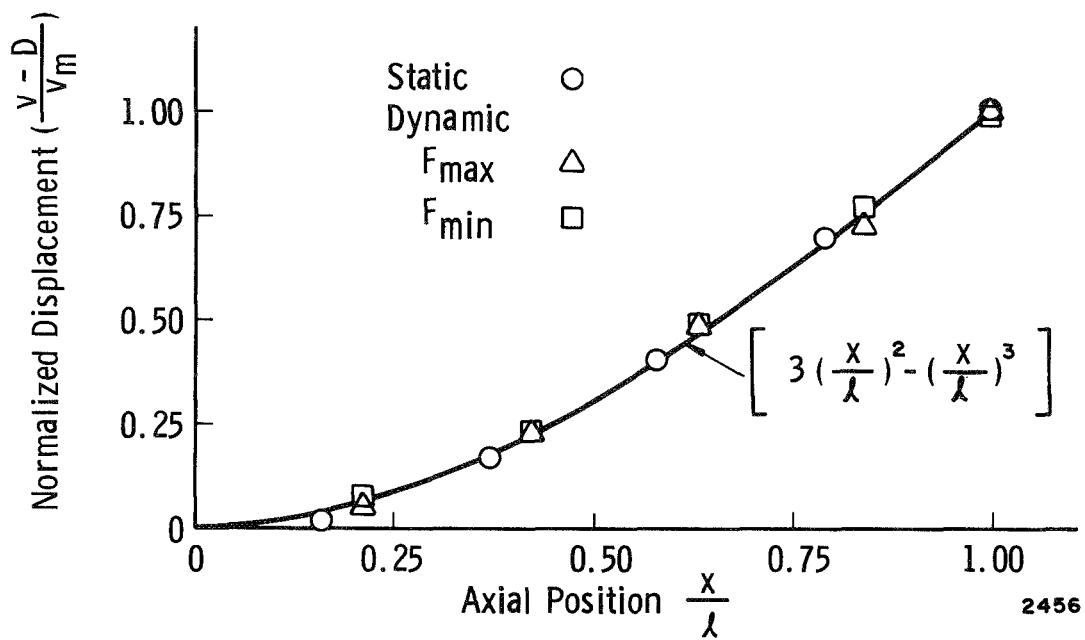


FIGURE 11. NORMALIZED STATIC AND DYNAMIC MODE SHAPES FOR CANTILEVER BEAM

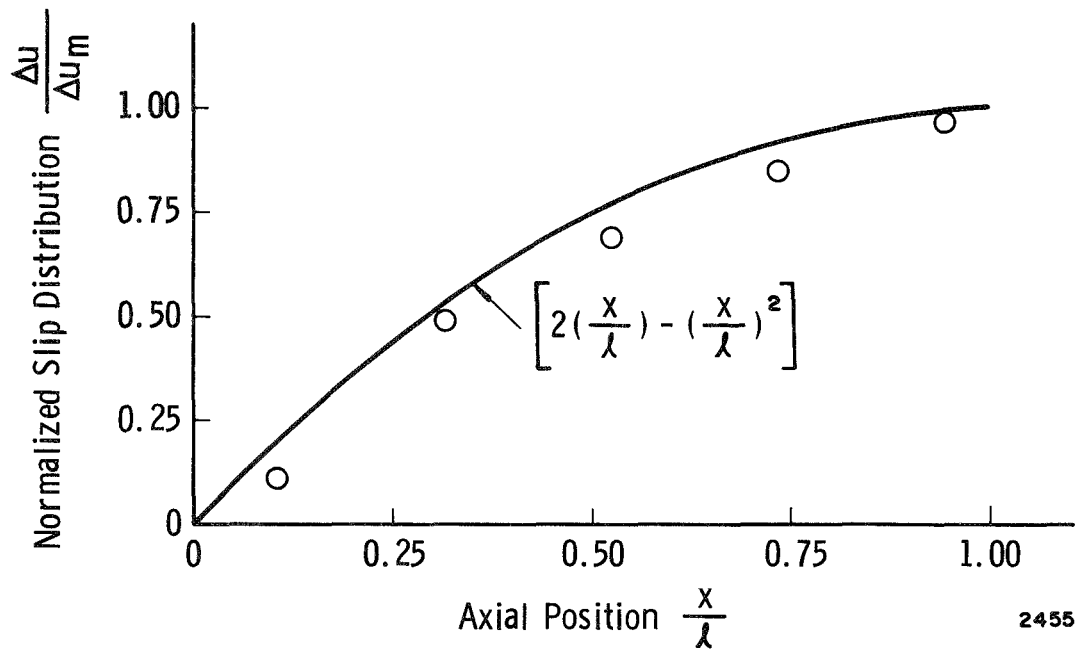


FIGURE 12. COMPARISON OF THEORETICAL AND DYNAMIC EXPERIMENTAL SLIP DISTRIBUTIONS FOR CANTILEVER BEAM

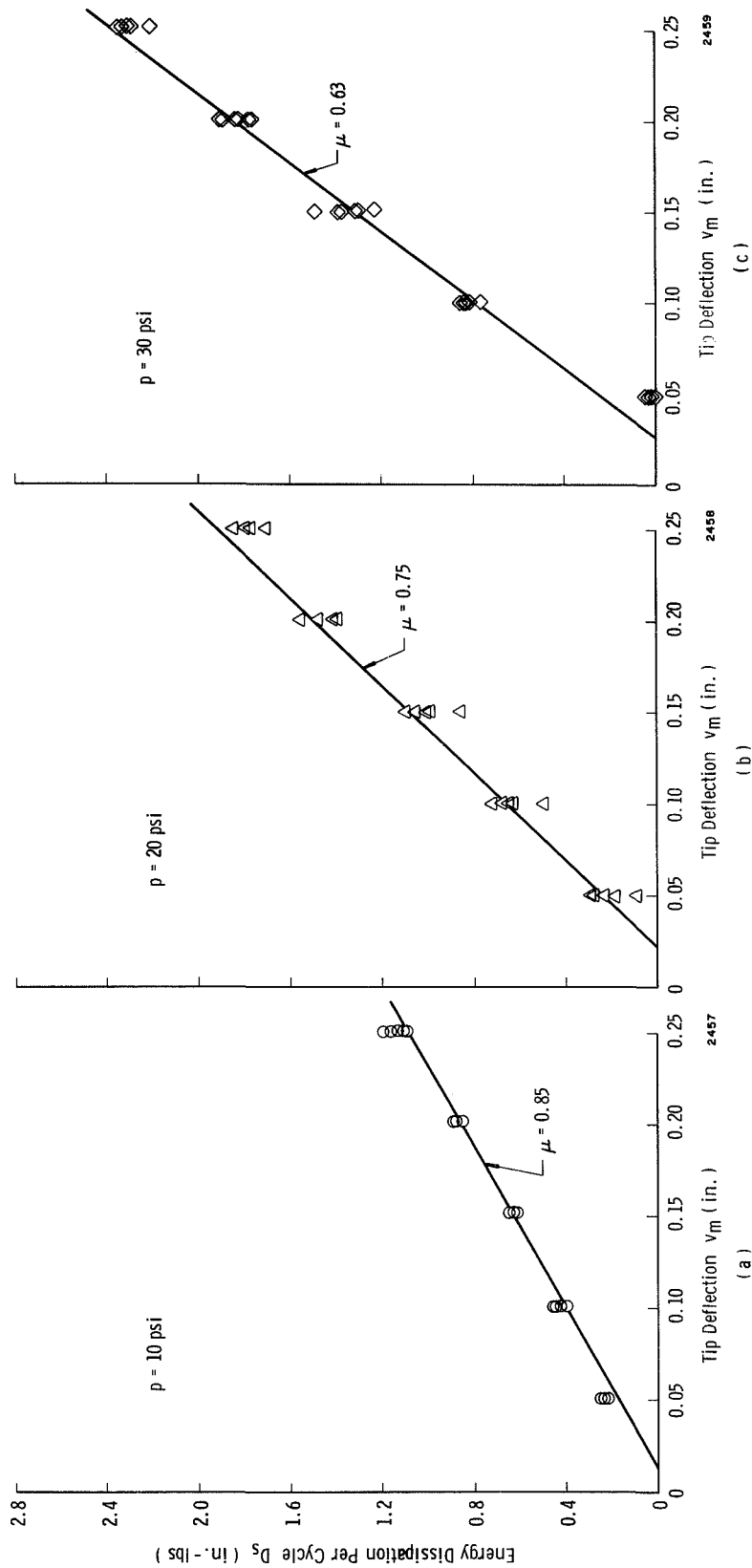


FIGURE 13. ENERGY DISSIPATION VS TIP DEFLECTION FOR BEAMS TESTED  
IN AIR UNDER LABORATORY CONDITIONS

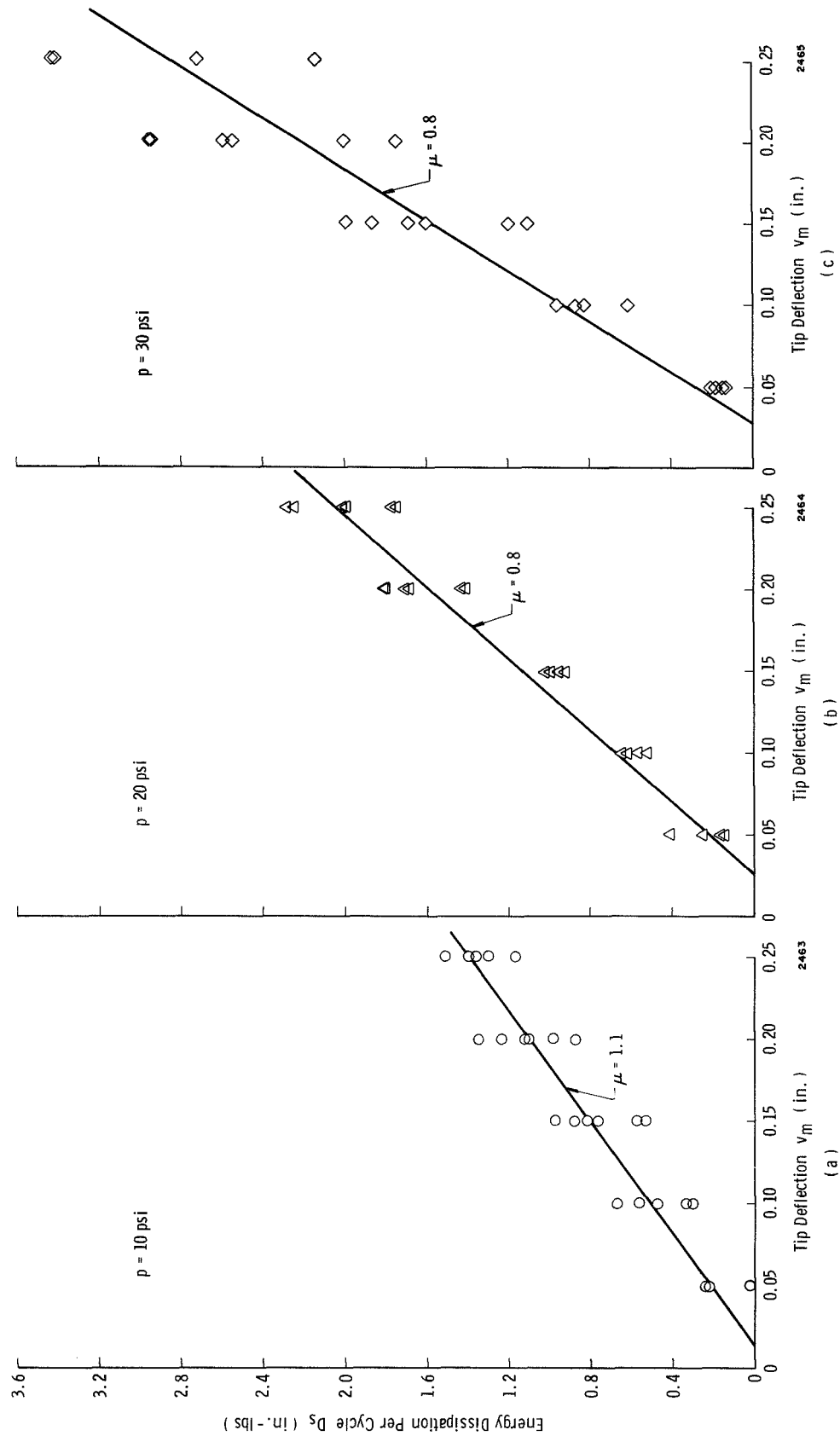


FIGURE 14. ENERGY DISSIPATION VS TIP DEFLECTION FOR BEAMS TESTED IN DRY, HYDROCARBON-FREE AIR

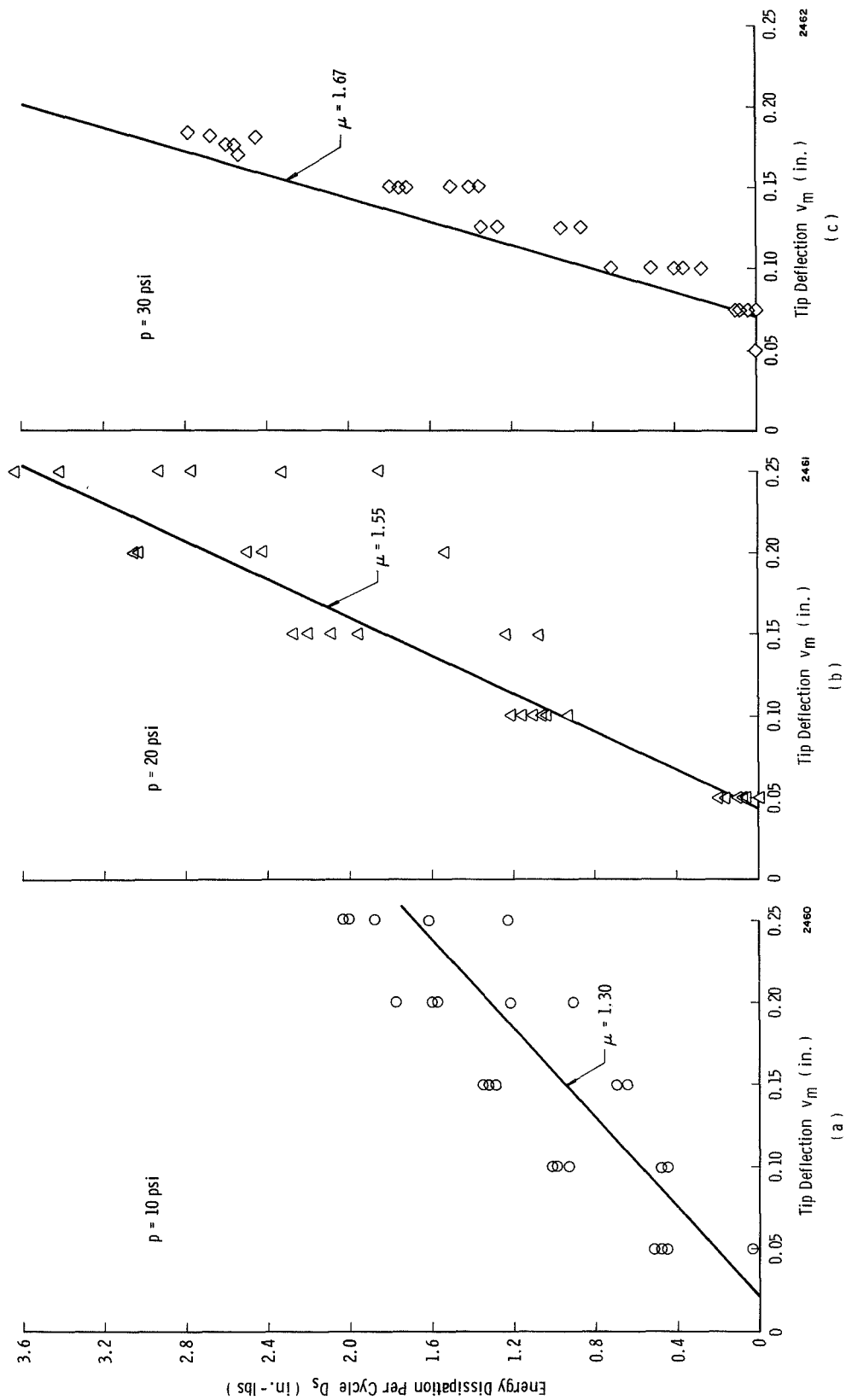


FIGURE 15. ENERGY DISSIPATION VS TIP DEFLECTION FOR BEAMS TESTED IN VACUUM ( $\approx 10^{-9}$  TORR)

TABLE I  
COEFFICIENT OF FRICTION  $\mu$ , DETERMINED  
FROM BEAM VIBRATION TESTS

Test Condition	Clamping Pressure (psi)		
	10	20	30
Air	0.85	0.75	0.63
Dry Air	1.10	0.80	0.80
Vacuum ( $\approx 10^{-9}$ torr)	1.30	1.55	1.67

contributes to the increased coefficient of friction. Examination of the surfaces tested in vacuum show very bright and shiny localized wear areas.

The beams tested in vacuum were more unstable in their amplitude response and tended in some instances to "freeze up." This tendency towards increased friction or seizure is commonly referred to as cold welding. With constant input force, the displacement amplitude of the vibrating beam would suddenly decrease as slip at the interface ceased because of seizure. An increased input force would be required to initiate slip again.

The accumulated data on energy dissipation are replotted in Figure 16 as the loss coefficient vs the deflection parameter  $Rv_m/Q$ . The data points cover the entire range of displacement, clamping pressure, and environment of the present tests. The solid curve is defined by (14b) and describes accurately the mean value of the data points. There is, of course, the same large deviations about the mean that appear in the previous energy dissipation data.

Figure 17 shows the variation in effective resonant frequency vs the deflection parameter  $Rv_m/Q$ . The solid curve is based upon (42) and shows that the ratio of the maximum to minimum resonant frequency is two to one. The actual frequency range was from 60 to 120 cps. These frequencies are lower than would be indicated by direct application of (42) because of the additional mass of the clamps on the experimental beams.

A final factor, which has not been discussed as yet, is the temperature rise of the beam resulting from the energy dissipated at the interface. Figure 18 shows the temperature-time history of a beam vibrating in air with a tip amplitude of 0.25 in. and with a clamping pressure of 30 psi. The measurement was made with a thermocouple mounted 1 in. from the tip on the outer surface of the beam. The beam shows a temperature rise of 40°F and approaches equilibrium in approximately 20 min. Of course, the energy is dissipated very locally at asperity contacts, and at these points the temperature may be somewhat higher. For a good thermal conductor, such as aluminum, the peak temperatures at the interface are probably not much greater than those measured. Significant thermal softening of 7075-T6 aluminum does not occur until above about 300°F.



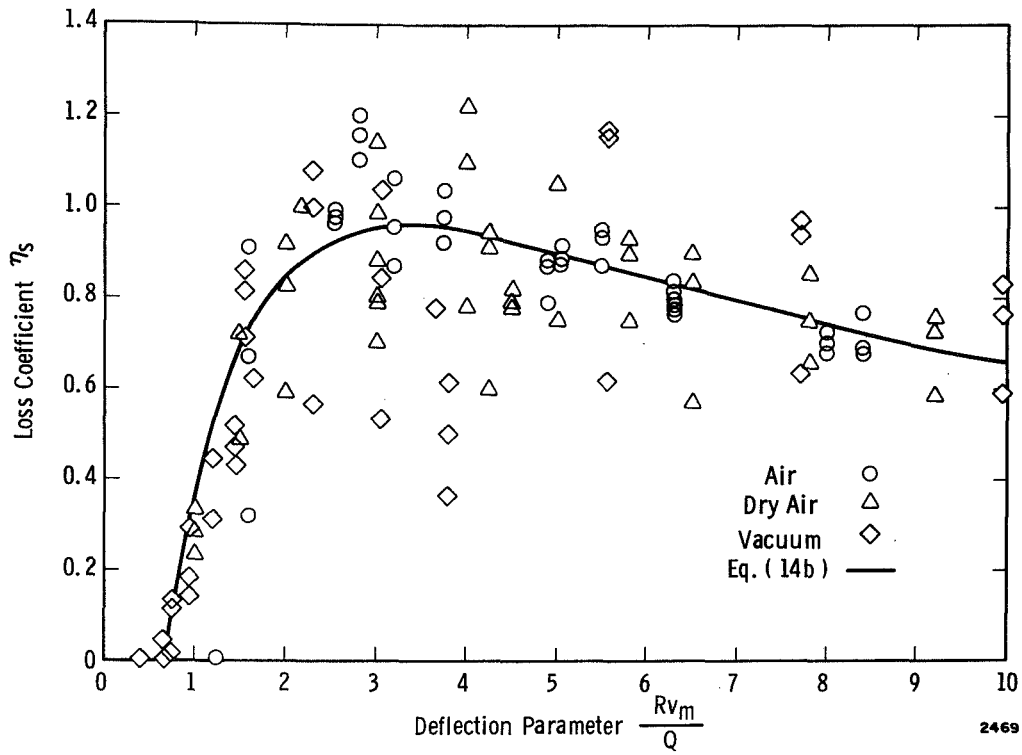


FIGURE 16. LOSS COEFFICIENT VS DEFLECTION PARAMETER FOR ALL TESTS

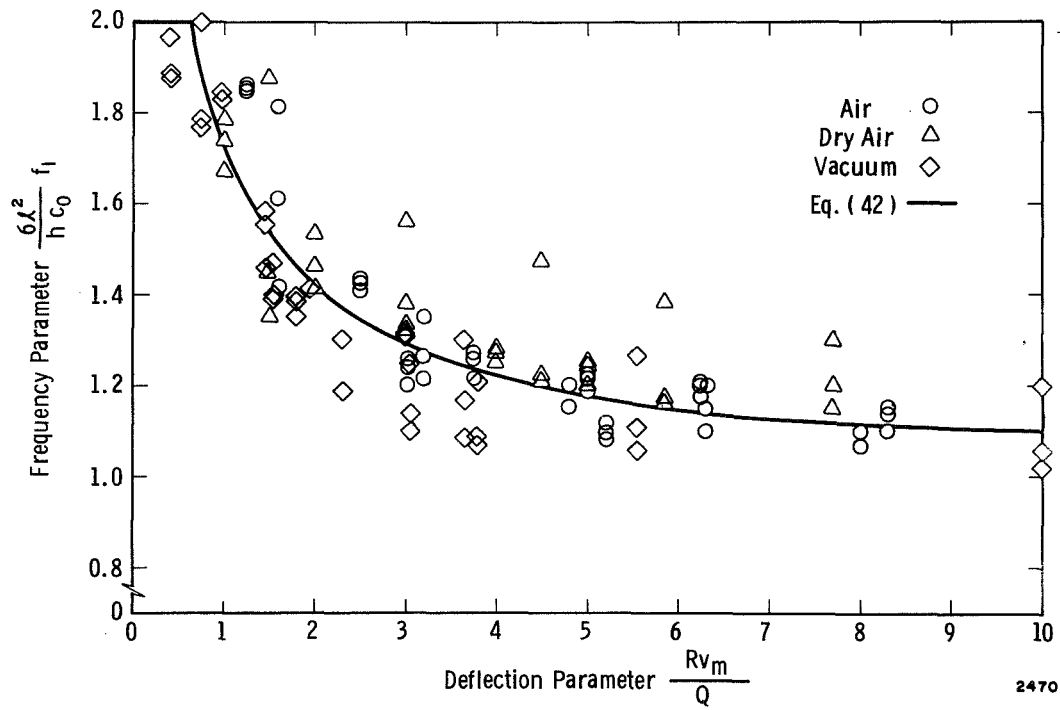


FIGURE 17. VARIATION OF THE APPARENT FIRST MODE FREQUENCY WITH THE DEFLECTION PARAMETER  $Rv_m/Q$

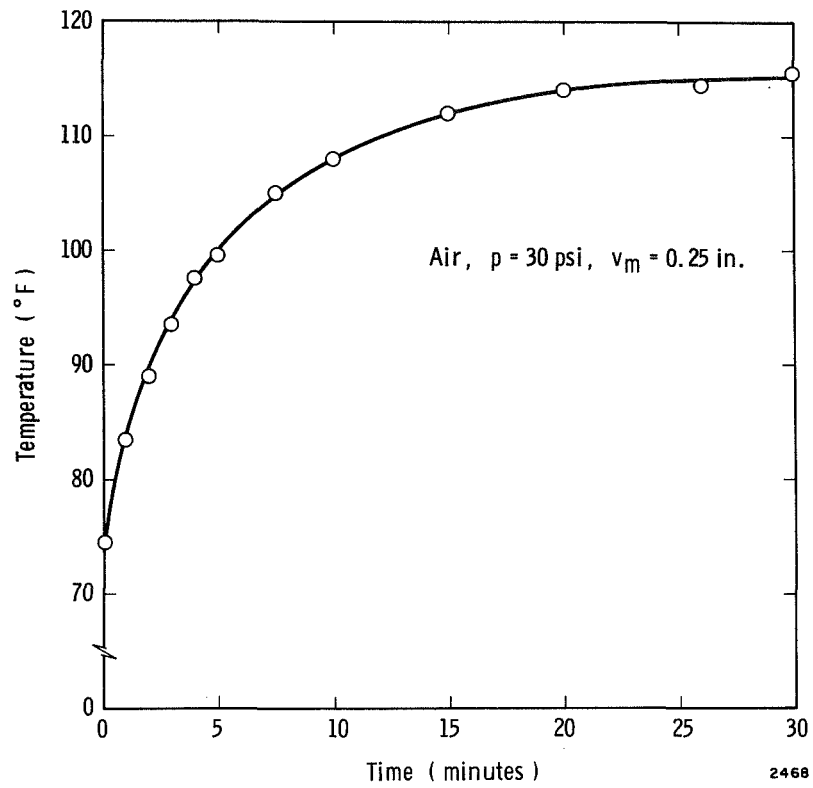


FIGURE 18. TEMPERATURE RISE MEASURED AT THE TIP OF CANTILEVER BEAM DURING STEADY VIBRATION

#### IV. OSCILLATORY SLIP EXPERIMENTS WITH COPPER

Oscillatory slip experiments were performed with copper in the same manner as previously reported for aluminum. [1] These experiments consist of measuring the oscillatory tangential force and relative displacement between two 1-in.-square blocks of the specimen material which are pressed together with a static normal load. Copper has an oxide of equivalent hardness as the base metal in contrast to the aluminum which forms a hard oxide. The hardness of aluminum and its oxide is 15 and 1800 Kg/mm<sup>2</sup>, respectively; the corresponding values for copper are 120 and 150 Kg/mm<sup>2</sup> [13]. The experiments with copper were intended to further clarify the role of surface oxides in controlling slip behavior in air and in vacuum. The copper specimens were run in the same apparatus as previously reported [1] and the measurements were made in essentially the same manner.

The surfaces of the copper specimens were machined with a flycutter in the same manner as the aluminum. The contacting surfaces were cleaned in the following steps: (1) cleaned in a vapor degreaser for 5 min, (2) put in a cathodic cleaner and heated to 140°F, (3) rinsed with tap water, (4) plated in a 50-percent hydrochloric acid, 50-percent distilled water solution for 1 min, and (5) finally rinsed in distilled water and ethyl alcohol. The chemical composition of the copper was: iron, 0.1 percent; phosphorous, 0.001 percent; oxygen, 0.021 percent; copper, 99.96 percent; other elements, nil.

The specimens were first tested at low tangential force increments in the microslip range.\* Hysteresis loops were recorded at each force increment. In all cases for microslip, the normal load was 20 lb and the frequency of the tangential force was 50 cps. The tangential force was then increased in magnitude to produce gross slip and the specimen was run in this condition for a period of approximately 4 hr. Subsequently, the tangential force was again reduced and the microslip measurements were repeated. Three specimens each were run in vacuum ( $<10^{-9}$  torr) and in dry air.

For displacements in the microslip range, compliance measurements indicated more scatter than in the aluminum because of the greater difficulty encountered in uniformly machining the copper surfaces and, perhaps, in obtaining equivalent surface cleanness. For the limited number of specimens tested, there appeared no significant difference in the initial compliance or in the compliance after gross slip between the specimens tested in air and those tested in vacuum. The copper specimens did show evidence of workhardening effects in that the microslip hysteresis loops closed up gradually in the initial period after application of tangential load. Measurements were taken only after 10 min of oscillation at each incremental load, or after the loops were stabilized.

Measured values of energy dissipation per cycle are given in Figures 19 and 20 for air and vacuum runs. For runs in both air and vacuum, the energy dissipation does not appear to be markedly changed between initial runs and runs made after gross slip had occurred. Both this result and the compliance data suggest that the oxide layer is playing less of a role than was apparent with the aluminum. For the aluminum, heavy mechanical wear produced by the prolonged gross slip was reflected in subsequent changes in the microslip compliance and dissipation. For equal tangential force amplitudes, the vacuum data do indicate lower energy dissipation values. This implies a greater resistance to slip and higher effective coefficient of friction for the tests in vacuum.

Typical gross slip hysteresis loops are shown in Figure 21. The shape of the microslip hysteresis loops were similar to the aluminum [1]. The gross slip loop obtained in air for copper also looks very similar to the corresponding loop for aluminum. The surfaces of copper specimens observed after gross slip in air showed the existence of dark oxide particles in the wear tracks as in the aluminum. Similar surfaces for tests performed in vacuum had bright or shiny wear tracks and no evidence of particles. In vacuum, the force during slip appears unstable and the loops are somewhat saddle-shaped. They are similar to loops obtained with aluminum after a period of slip in nitrogen (Ref. 1, Figure 22). The saddle shape may indicate a difference in the static and dynamic coefficient of friction.

---

\*Tangential loads less than required to produce gross slip or relative rigid body displacements between the two surfaces.

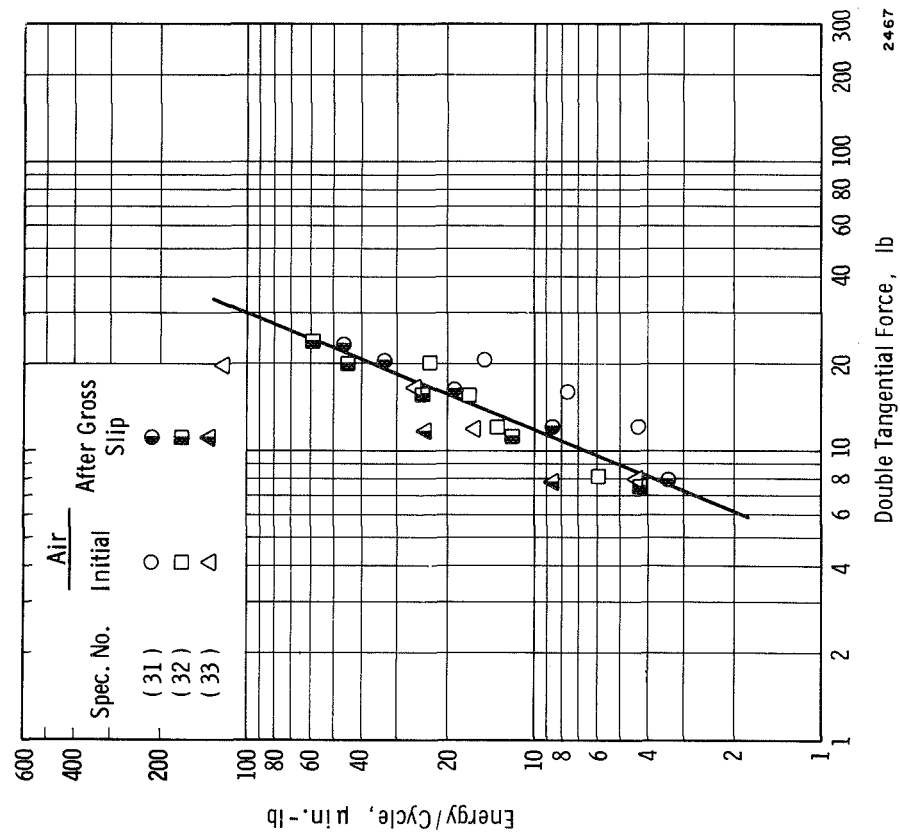


FIGURE 19. ENERGY DISSIPATION VS TANGENTIAL FORCE  
FOR COPPER TESTS IN AIR

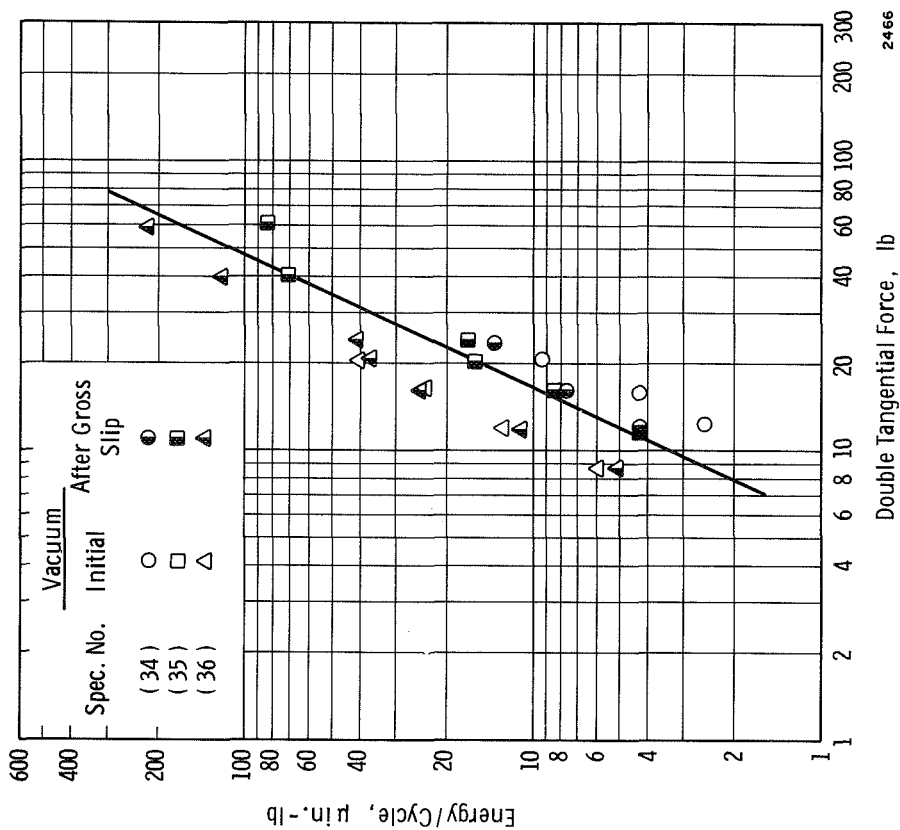


FIGURE 20. ENERGY DISSIPATION VS TANGENTIAL FORCE  
FOR COPPER TESTS IN VACUUM

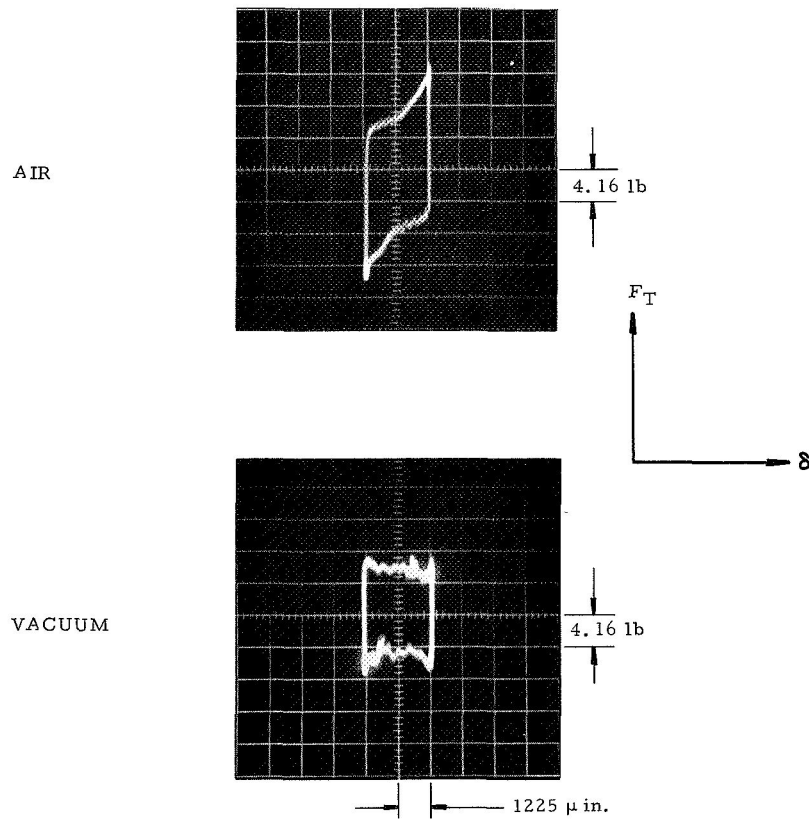


FIGURE 21. GROSS SLIP HYSTERESIS LOOPS FOR COPPER  
IN AIR AND IN VACUUM

The gross slip measurements gave a very large change in apparent coefficient of friction between air and vacuum runs. In Figure 21, the tangential force required to initiate slip is approximately the same in both the air and vacuum records. However, while the normal force in the air test is 10 lb, it was necessary to reduce the normal force to 1 lb in the vacuum tests in order to produce slip. The coefficient of friction determined from the ratio of the tangential force required to initiate gross slip to the force normal to the surface was 0.52 in air and 7.15 in vacuum, an order of magnitude difference.

It appears that, while the influence of the oxide on copper may not be as significant as with aluminum, other surface or material properties are causing a much stronger vacuum adhesion or welding with copper than with the aluminum.

## V. DISCUSSION

The experiments on beam damping were compared with analysis which included only the slip mechanism for dissipation of energy. Other dissipation mechanisms are present, the most significant of which are air damping and internal material damping due to cyclic stressing. Baker, et al. [14] have examined these mechanisms in detail for cantilever beams. For air damping, the primary mechanism appears to be a drag force proportional to the square of the velocity of the beam. The loss coefficient can be given for this mechanism by

$$\eta_{SA} = \frac{4}{3\pi} \frac{\rho_A}{\rho} C_D \beta_n \frac{v_m}{2h}$$

where  $\rho_A/\rho$  is the ratio of the density of air to that of the beam,  $C_D \simeq 1$  is a drag coefficient,  $\beta_n$  is a parameter related to the beam mode shape ( $\beta_1 = 1.473$ ) and  $2h$  is the thickness of the beam. Substituting appropriate values gives  $\eta_{SA} = (5 \times 10^{-4}) v_m/2h$ , which for the entire range of the present experiments is negligible with respect to the slip mechanism.

Material damping may arise from several internal mechanisms in metals. However, the dominant mechanism at low frequencies appears to be Zener type damping which is based upon a viscoelastic solid with complex modulus and a relaxation time based upon transverse heat flow. The loss coefficient for this mechanism is given by [12,14]

$$\eta_{SM} = \frac{\alpha^2 ET}{C} \frac{\omega\tau}{1 + \omega^2\tau^2}$$

where

$\alpha$  = linear thermal expansion coefficient

$E$  = Young's modulus

$T$  = absolute temperature

$C$  = specific heat

$\omega$  = frequency of harmonic motion

$\tau$  =  $h^2 c / \pi^2 k$  = relaxation time

$k$  = thermal conductivity

$h$  = beam thickness

The maximum in  $\eta_{SM}$  occurs when  $\omega\tau = 1$ . For aluminum, the maximum value is approximately  $2.4 \times 10^{-3}$ . For the beams used in the present experiments, this maximum in loss coefficient occurs at a frequency of about 3 cps. At 60 cps, the lowest frequency used, the loss coefficient is down about one order of magnitude, again negligible compared with the loss coefficient due to slip.

It is apparent that slip damping can be a dominant contributor to the overall damping of structures or assemblies which contain joints under load. In a vacuum or space environment, where there is the loss of the various air damping mechanisms, slip damping can be even more significant. Therefore, one of the objectives of the present program was to evaluate to what extent slip damping itself would be affected by vacuum conditions. From the analysis, for which the basic assumptions appear to be verified by the present experiments and those of previous investigators, it is evident that

any effect which alters the coefficient of friction of the surfaces in contact will change the energy dissipation or the loss coefficient. Studies of friction in vacuum are fairly extensive and generally indicate an increase in  $\mu$  over ambient conditions. The magnitude of this increase is, of course, dependent upon the specific material and its surface and bulk properties.

The answer to the question of whether the damping or loss coefficient will increase or decrease for a given structure taken from an air to a vacuum environment depends upon too many parameters to answer directly. For structures analogous to the one studied herein, it is obvious from Figure 3 that the loss coefficient may either increase or decrease with increasing coefficient of friction depending upon the value of the parameter  $R\nu_m/Q$ . Since this parameter contains five other variables in addition to the friction coefficient, it is possible to discuss the effects of  $\mu$  alone only if the other parameters are fixed. The loading or displacement is usually not fixed. It should also be observed that not all systems containing slip elements will behave as in Figure 3 or have a maximum in  $\eta_S^*$ . Analysis is needed for a wider range of structural systems with slip.

However, when the other system parameters are fixed and an analysis, such as derived herein, is available, the effect of changing friction coefficient can be quantitatively established. In applications, a major problem will be establishing an accurate value for the friction coefficient. The present tests demonstrate that this is not a very reproducible parameter. This is especially true for unlubricated, microscopically rough surfaces. Since the asperity contact is essentially random, the mechanics of the interface under load is not completely deterministic. Therefore, the same load-deflection characteristics are not obtained for two interfaces which may be otherwise macroscopically similar. It should be noted that the average coefficients of friction obtained from the present beam bending tests are higher, both for air and vacuum tests, than those previously reported [1] for tangential slip experiments with small blocks having surfaces prepared in the same manner. These again may be different from values obtained from standard friction tests using small spherical contact areas because of the differences in contact geometry. This is a perplexing problem for the designer or analyst who has the responsibility of predicting system performance.

There are two directions in which research in interfacial slip is proceeding. The first is concerned with the detailed analysis of the mechanics of rough surface contact, with the objective of establishing a quantitative theory for slip in terms of the surface geometry and the surface and bulk properties of the materials. This direction is exemplified by the studies of Greenwood and Tabor [15] and Edwards and Halling [16,17]. The second direction is the engineering approach to establish the overall loss properties of various types of joints and connections found in structural systems. These analyses, such as the one presented herein, are based upon the assumption that slip is governed by Coulomb friction. A number of such studies were referenced in the introduction.

The solutions available with the engineering approach are limited. They are restricted to simple lap joints under uniform axial force or torsion for bushing type joints and the few examples of beam bending already cited. Specific problems for flexural members which should be further examined include the effects of spatially variable normal pressure at the interface, more complex distributions of the applied loading, more exact solutions for distributed inertia loads, other boundary conditions for beams, and two-dimensional slip situations such as might occur with plates or shells. These solutions would help to place bounds on the magnitude of the loss coefficient and its variation with load or deflection for particular types of structural configurations.

For example, the upper bound on the loss coefficient for the system studied in this report is very high, much higher than usually found in structural systems. This is because, in this example, the slip area encompasses the entire structure (beam) and the in-plane slip motion is unrestricted. For more general cases, the slip area is smaller with respect to the overall dimensions of the structure and the in-plane slip displacements are constrained at periodic intervals by rivets, bolts, or rigid terminations of some sort. These factors can significantly reduce the ratio of energy dissipation to elastic energy storage capacity.

---

\*See, for example, Lazan [10], p 114.

In practice, prediction of interface damping capacity is still restricted to relatively simple slip systems where the boundary and loading conditions are well prescribed. Even in these cases, unless the interface is specially prepared, variability in the friction coefficient will lead to uncertainty in quantitative values. Also, one should keep in mind the inherent nonlinearity and hysteretic nature of the system when slip occurs. Nevertheless, the basic analysis has been established and verified by experiments on simple structures. Analysis of more complex systems is now needed to provide a more general understanding of the influence of structural parameters on interface damping capacity.



## VI. CONCLUSIONS

The following conclusions have been derived from the analysis and experiments described in this report:

- (1) The loss coefficient for a cantilever beam including slip can be expressed in terms of a single nondimensional displacement parameter. The loss coefficient has a maximum at a finite value of this parameter.
- (2) Solutions for slip in cantilever beams previously available have been extended to beams with either nonsymmetric or multiple interfaces.
- (3) To a first approximation, the inclusion of distributed inertia loading does not change the energy dissipated per cycle for a beam in forced vibration when compared with an equivalent static maximum deflection of the same beam. The deflection mode shape and the axial distribution of slip is modified, however.
- (4) The change in frequency with amplitude of a cantilever beam including slip can be predicted.
- (5) From vibration experiments with aluminum beams having an interface under uniform clamping pressure, the coefficient of friction is appreciably greater in vacuum than in air. This may lead to either an increase or a decrease in the loss coefficient depending upon the displacement amplitude and other physical parameters of the beam.
- (6) Slip experiments with copper blocks in air and vacuum did not show as much effect of the wear of the oxide layer as did aluminum specimens previously tested. However, the apparent coefficient of friction for copper was much greater in vacuum than in air.

## VII. REFERENCES

1. U. S. Lindholm, R. D. Brown, and L. M. Yeakley, "Studies of Interface Damping," Summary Tech. Rept. No. 1, Contract NAS5-10310 (1968).
2. L. E. Goodman, "A Review of Progress in Analysis of Interfacial Slip Damping," **Structural Damping**, J. Ruzika, Ed., ASME, New York (1959).
3. S. W. E. Earles, "Theoretical Estimation of the Frictional Energy Dissipation in a Simple Lap Joint," *J. Mech. Eng. Sci.*, Vol 8, p 207 (1966).
4. A. F. Metherell and S. V. Diller, "Instantaneous Energy Dissipation Rate in a Lap Joint-Uniform Clamping Pressure," *J. Applied Mechanics*, Vol 35, pp 123-28 (1968).
5. C. B. Brown, "Factors Affecting the Damping in a Lap Joint," **Proc. ASCE, J. Struc. Div.**, Vol 94, ST5, p 1197 (1968).
6. T. H. H. Pian and F. C. Hallowell, Jr., "Structural Damping in a Simple Built-Up Beam," **Proc. 1st U. S. Natl. Cong. of Applied Mechanics**, pp 97-102, June 1951.
7. L. E. Goodman and J. H. Klumpp, "Analysis of Slip Damping with Reference to Turbine-Blade Vibration," *J. Appl. Mech.*, Vol 23, p 421 (1956).
8. T. H. H. Pian, "Structural Damping of a Simple Built-Up Beam with Riveted Joints in Bending," *J. Appl. Mech.*, Vol 24, pp 35-8 (1957).
9. R. R. McWithey and R. J. Hayduk, "Damping Characteristics of Built-Up Cantilever Beams in a Vacuum Environment," NASA TN-D-3065, November 1965.
10. B. J. Lazan, **Damping of Materials and Members in Structural Mechanics**, Pergamon Press (1968).
11. S. Timoshenko, **Vibration Problems in Engineering**, Van Norstrand Co, Inc, 3rd Edition, p 371 (1955).
12. N. Granick and J. E. Stern, "Material Damping of Aluminum by Resonance-Dwell Technique," *Shock and Vibration Bulletin* Vol 34, Part 5, pp 177-95 (1965).
13. F. P. Bowden and D. Tabor, **The Friction and Lubrication of Solids**, Part II, Oxford University Press, London (1964).
14. W. E. Baker, W. E. Woolam, and D. Young, "Air and Internal Damping of Thin Beams," *Int. J. of Mech. Sci.*, Vol 9, pp 743-66 (1967).
15. J. A. Greenwood and D. Tabor, "Deformation Properties of Friction Junctions," **Proc. Phys. Soc.**, Vol 68B, p 609 (1956).
16. C. M. Edwards and J. Halling, "An Analysis of the Plastic Interaction of Surface Asperities and Its Relevance to the Value of the Coefficient of Friction," *J. Mech. Eng. Sci.*, Vol 10, p 101 (1968).
17. C. M. Edwards and J. Halling, "Experimental Study of the Plastic Interaction of Model Surface Asperities During Sliding," *J. Mech. Sci.*, Vol 10, p 121 (1968).